https://dx.doi.org/10.1016/j.jlumin.2020.117488

This is the Pre-Published Version.

Structural modification of nonspecific thiazole orange for ligand-DNA interaction study: Understanding the ligand recognition selectivity towards G4-DNA over duplex-DNA

Yiwen Zhu [a,‡], Jinqiang Hou [d,‡], Xuan-He Huang [c], Dong-Xiao Zhong [c], Wei Long [c], Wenjie Liu [d], Yu-Jing Lu [c], Kun Zhang [e], and Wing-Leung Wong [b,e,*]

[a] College of Materials and Environmental Engineering, Hangzhou Dianzi University, Hangzhou, 310018, P. R. China.

[b] The State Key Laboratory of Chemical Biology and Drug Discovery, Department of Applied Biology and Chemical Technology, The Hong Kong Polytechnic University, Hung Hom, Kowloon, Hong Kong, China.

[c] Institute of Natural Medicine and Green Chemistry, School of Chemical Engineering and Light Industry, Guangdong University of Technology, Guangzhou 510006, P. R. China.

[d] Department of Chemistry, Lakehead University and Thunder Bay Regional Health Research Institute, 980 Oliver Road, Thunder Bay, On, P7B 6V4, Canada.

[e] School of Biotechnology and Health Sciences, Wuyi University, Jiangmen 529020, P.R. China; and International Healthcare Innovation Institute (Jiangmen), Jiangmen 529040, P.R. China.

‡ The authors contributed equally to this work.

* Corresponding author

E-mail: wing.leung.wong@polyu.edu.hk

© 2020. This manuscript version is made available under the CC-BY-NC-ND 4.0 license http://creativecommons.org/licenses/by-nc-nd/4.0/.

Abstract

The study of ligand interactions with nucleic acid structures such as G-quadruplexes versus double-stranded DNA is important because these interactions are fundamental for many intracellular processes. In the investigation of ligand-DNA binding process, achieving high fluorescent signal discrimination with strong binding affinity is challenging. To develop binding ligands with excellent recognition ability towards G4-DNA over duplex-DNA, the design of appropriate molecular scaffolds that are able to match with the G4-DNA binding pocket (G-quartet) is crucial. In the present study, the new fluorescent DNA binding ligands were designed and synthesized through the integration of a small and conjugated substituent group at the 2-position of the 1-methylquinolinium moiety of the nonspecific thiazole orange scaffold. The ligands were investigated in fluorescence binding assays and showed different interaction properties and significant fluorescent recognition selectivity towards G4-DNA over duplex-DNA *in vitro*. Molecular docking study of the ligands in complex with telo21 G4-DNA and ds26 duplex DNA revealed different binding modes. In addition, the cytotoxicity of the fluorescent DNA binding ligands was evaluated in MTT assays against two selected cancer cell lines (human prostate cancer cell (PC3) and human hepatoma cell (hepG2)). The IC_{50} was found in the range of 6.3–12.5 μM, indicating a relatively high cytotoxicity of the ligands towards the cancer cells examined.

Keywords: Fluorescent binding ligand, Ligand-DNA interaction, G-quadruplex DNA recognition, Molecular docking

1. Introduction

Deoxyribonucleic acid (DNA) is a vital genetic material for all life in nature as it takes various critical biofunctions in the growth, development, reproduction, heredity and variation of organisms. The classical topology of DNA is a double helical structure, which is intertwined by two complementary single strands and was first proposed by Watson and Crick in 1953.[1] Over the past decades, it has been discovered that DNA can form a number of non-canonical structures that do not follow the simple A-T and G-C base pairings, typical examples including hairpins and cruciforms, triplex-forming oligonucleotides, *i*-motif structures and G-quadruplexes (G4).[2, 3] Interestingly, the guanine (G)-rich DNA sequences that are capable of forming G4-structures in human are found highly concentrated at the regions of telomere repeats (at the chromosomal extremities) and oncogenic promoters (at the intra-chromosomal region).[4, 5] Recent evidences also suggest that G4-structures may have important biological functions at cellular level such as the regulatory roles in the expression of certain human oncogenes, such as c-myc, c-kit and K-ras, and the perturbation of telomere replication.[6-8] It has been shown that enhancing the formation and stabilization of telomeric G4-DNA structures *in vivo* may inhibit the telomerase activity in telomere extension in cancer cells.[9-11] Currently, DNA G-quadruplexes have been considered as a potential target for drug design.[12-14] Therefore, it is of great importance to design and develop novel and G4-specific small organic binding ligands for the *in vivo* recognition and stabilization of G4-structures.

Many bioinformatics studies showed that about 376,000 possible G4 formation sequences (putative quadruplex sequences) in the human genome appear to correlate with functional genomic regions.[13, 15, 16] However, to distinguish G4-DNA structures from large amounts of double-stranded DNA and/or other form of nucleic acid structures *in vivo* with small binging ligands is challenging.[13] Nonetheless, with the use of G4-specific fluorescent binding ligands [17-28], the study of their biofunctions, structural folding dynamics and the real-time location of appearance *in vivo* can be possible. In recent years, a variety of G4-DNA targeting fluorescent probes have been reported and reviewed.[12, 17-29] Some typical examples such as benzothiazole [24] and thioflavin T [30], naphthalene diimide [31], triphenylamine [32], triaryl-substituted imidazole[11], quinolinium [33-35], thiazole orange derivatives [36-38], carbazole derivative [39], porphyrin dyes [40] and triphenylmethane [41] are found possessing good selectivity towards G4-DNA over duplex-DNA. For the study of ligand-DNA interaction *in vitro* or *in vivo*, in order to achieve merit fluorescent signal discrimination and display higher affinity to interact with G4-DNA over duplex-DNA, the design of molecular scaffolds that are able to match with the G4-DNA binding pocket (G-quartet) is crucial.

Some recent reports revealed that the feature of a binding ligand such as molecular shape [42], symmetry [43, 44], the planarity and polarity of ligands [12, 45, 46] and the electronic effect of terminal groups [47-49], may have significant influence in the ligand–G4-DNA interaction specificity and affinity. In the present study, three new G4-DNA binding ligands based on a relatively rigid thiazole orange (TO) scaffold were synthesized by varying the molecular size and flexibility of the terminal substituent groups for probing the interaction characteristics of the G-quartet of telomeric G4-DNA because the understanding of binding site matching in rational drug design is essential.[50] These new fluorescent ligands investigated in a number of binding assays showed different interaction properties and good fluorescent discrimination towards G4-DNA structures over duplex DNA. Molecular docking study of the ligands in complex with telo21 G4-DNA and ds26 duplex DNA was also performed for comparison.

2. EXPERIMENTAL SECTION

2.1 Materials and instrumentation

All chemicals were purchased from commercial sources unless otherwise specified. All the solvents were of analytical reagent grade and were used without further purification. All oligonucleotides used in this work were synthesized and purified by Shanghai Sangon Biotechnology Co. Ltd. (Shanghai, China). The sequences were listed in Table S1. Fluorescence studies were performed with a LS45 luminescence spectrophotometer (Perkin-Elmer, USA). A quartz cuvette with 2 mm x 2 mm path length was used for the spectra recorded at 10 nm slit width for both excitation and emission unless otherwise specified. Mass spectra (MS) were recorded on Bruker amaZon SL mass spectrometer with an ESI or ACPI mass selective detector. ^{1}H and ^{13}C NMR spectra were recorded using TMS as the internal standard in $CDCl_3$ or DMSO-d_6 with a Bruker BioSpin GmbH spectrometer at 400 MHz and 100 MHz, respectively. The purity of synthesized compounds was confirmed by using analytical HPLC with a dual pump Shimadzu LC-20A system equipped with a photo-diode array detector and a C18 column (250 mm x 4.6 mm, 5 µM YMC) and eluted with acetonitrile/water (47:53) containing 0.5 % acetic acid at a flow rate of 1.0 mL/min. The stock solutions of the ligands were prepared at 5 mM with DMSO. The stock solution was then diluted to the required concentration with Tris–HCl buffer containing 60 mM KCl for experiments. All the titration experiments, binding studies, FRET assays and bioassays were repeated in triplicate.

2.2 General procedures for the synthesis of new DNA binding ligands

The starting compound (*Z*)-1,2-dimethyl-4-((3-methylbenzo[d]thiazol-2(3H)-ylidene)methyl)quinolin-1-ium iodide was obtained by followed the reported procedures.[37] The intermediate compound (0.16 mmol) was then further reacted with the selected aromatic aldehyde (0.32 mmol, benzaldehyde, or 2-naphthaldehyde or *trans*-cinnamaldehyde) using 4-methylpiperidine (0.5 mL) as a base and *n*-butanol (10 mL) as the solvent. The mixture was well-mixed at room temperature and then was heated to reflux for 3 h. After reaction, the mixture was cooled in an iced-bath and the precipitates were collected by suction filtration. The solid was further washed with *n*-butanol. The crude product was purified by using flash column chromatography to afford the desired pure compounds. These new compounds were characterized unambiguously with ^{1}H and ^{13}C NMR, ESI-MS and HPLC before utilized for fluorescence analysis and bioassays.

2.3 Characterization of the DNA binding ligands 1-3

Ligand 1: 1-methyl-4-((Z)-(3-methylbenzo[d]thiazol-2(3H)-ylidene)methyl)-2-((E)-styryl) quinolin-1-ium iodide was obtained as dark red solid with yield 85 %. Melting point: 230-234 ^{o}C. ^{1}H NMR (400 MHz, DMSO) δ 8.76 (d, *J* = 8.2 Hz, 1H), 8.17 (d, *J* = 8.2 Hz, 1H), 8.06 (t, *J* = 8.6 Hz, 1H), 7.99 (m, 1H), 7.94 (m, 2H), 7.76 (m, 3H), 7.67 (s, 1H), 7.63 – 7.57 (m, 2H), 7.56 – 7.47 (m, 3H), 7.39 (t, *J* = 8.6 Hz, 1H), 6.90 (s, 1H), 4.15 (s, 3H), 3.99 (s, 3H). ^{13}C NMR (101 MHz, DMSO) δ 160.06, 152.47, 148.36, 141.20, 141.05, 139.54, 135.70, 133.77, 130.71, 129.43, 128.90, 128.56, 126.99, 125.73, 124.74, 124.33, 124.04, 123.48, 122.35, 119.03, 113.20, 108.58, 88.43, 38.58, 34.19. ESI-MS for $[M–I]^{+}$ ($C_{28}H_{25}N_2S^{+}$): calculated m/z = 407.2, found m/z = 407.0. HPLC retention time with an eluent CH_3CN: 0.5% $CH_3COOH_{(aq)}$ = 53:47 (v/v) was 4.89 min. The purity of the compound was higher than 95 %.

Ligand 2: 1-methyl-4-((Z)-(3-methylbenzo[d]thiazol-2(3H)-ylidene)methyl)-2-((E)-2-(naphth aalen-2-yl)vinyl)quinolin-1-ium iodide was obtained as black solid with 85 %. Melting point: 299-304 ^{o}C. ^{1}H NMR (400 MHz, DMSO) δ 8.78 (m, 1H), 8.41 (s, 1H), 8.18 (t, *J* = 8.6 Hz, 2H), 8.11 – 8.04 (m, 2H), 8.01 (m, 3H), 7.91 (s, 1H), 7.85 (s, 1H), 7.75 (t, *J* = 8.6 Hz, 2H), 7.67 (s, 1H), 7.65 – 7.56 (m, 3H), 7.40 (m, 1H), 6.94 (d, *J* = 7.4 Hz, 1H), 4.20 (s, 3H), 3.99 (s, 3H). ^{13}C NMR (100 MHz, DMSO) δ 159.99, 152.42, 148.28, 141.24, 141.06, 139.55, 134.15, 133.76, 133.39, 133.34, 130.41, 129.05, 128.89, 128.56, 128.30, 127.90, 127.44, 126.99, 125.73, 124.72, 124.58, 124.32, 124.05, 123.52, 122.55, 119.06, 113.19, 108.52, 88.44, 38.63, 34.18. ESI-MS for $[M–I]^{+}$ ($C_{31}H_{25}N_2S^{+}$): calculated

m/z = 457.2, found m/z = 457.0, HPLC retention time with an eluent CH_3CN: 0.5% $CH_3COOH_{(aq)}$ = 53:47 (v/v) was 6.90 min. The purity of the compound was higher than 95 %.

Ligand 3: 1-methyl-4-((Z)-(3-methylbenzo[d]thiazol-2(3H)-ylidene)methyl)-2-((1E,3E)-4-phenylbuta-1,3-dien-1-yl)quinolin-1-ium iodide was obtained as a dark brown solid with 79 %. Melting point: 254-257 ºC. ^{1}H NMR (400 MHz, DMSO) δ 8.73 (m, 1H), 8.10 (dd, *J* = 12, 6 Hz, 2H), 7.97 – 7.92 (m, 1H), 7.74–7.68 (m, 2H), 7.67–7.61 (m, 2H), 7.60–7.51 (m, 3H), 7.45 (dd, *J* = 12, 6 Hz, 2H), 7.42–7.35 (m, 3H), 7.31 (m, 2H), 6.83 (d, *J* = 7.4 Hz, 1H), 4.06 (s, 3H), 3.97 (s, 3H). ^{13}C NMR (100 MHz, DMSO) δ 159.64, 151.84, 147.88, 141.95, 141.06, 140.24, 139.50, 136.52, 133.65, 129.66, 129.53, 128.60, 128.54, 127.64, 126.90, 125.64, 125.09, 124.64, 124.24, 123.96, 123.48, 118.98, 113.11, 108.00, 88.23, 38.24, 34.12. ESI-MS for $[M–I]^+$ ($C_{29}H_{25}N_2S^+$): calculated m/z = 433.2, found m/z = 433.2. HPLC retention time with an eluent CH_3CN: 0.5% $CH_3COOH_{(aq)}$ = 53:47 (v/v) was 1.70 min. The purity of the compound was higher than 95 %.

2.4 Fluorescent quantum yields

The fluorescent quantum yields of the binding ligands in the presence of DNA were calculated using fluorescein in 0.1 N NaOH ethanol as standard (Φ = 0.85).[51] Absorbance and fluorescence values were recorded after adding five solutions with an increasing concentration of a selected sample into fixed a concentration of DNA solution. Quantum yields were calculated according to the equation [52]: $\Phi_x = \Phi_{ST}\,(Grad_x / Grad_{ST})\,(\eta^2_x / \eta^2_{ST})$; where the subscripts ST and X denote the standard and test respectively; Φ is the fluorescence quantum yield; Grad is the gradient from the plot of integrated fluorescence intensity versus absorbance, and is the refractive index of the solvent.

2.5 Fluorescence binding assays

In the fluorescence titration experiments, the excitation wavelength (λ_{ex}) used was 510 nm and the emission wavelength (λ_{em}) **1**, λ_{em} = 620 nm; **2**, λ_{em} = 530 nm and **3**, λ_{em} = 550 nm. For fluorescence titration assays, the final concentration of the binding ligand used was fixed at 5 μM in a Tris–HCl buffer containing 60 mM KCl. Measurements were taken after incubated for 10 min at 25 °C. With the data obtained through fluorimetric titrations, the binding constants were analyzed according to the independent site model by nonlinear fitting to the equation [53]: $F/F_0 = 1+(Q-1)/2$, where F_0 is the fluorescence intensity of **1–3** in the absence of DNA, F_{max} is the fluorescence intensity upon saturation of DNA, $Q = F_{max}(F_0)^{-1}$, $A = (K_{eq}C_{dye})^{-1}$, and $x = nC_{DNA}(C_{dye})^{-1}$; *n* is the putative number of binding sites on a given DNA matrix. The parameters Q and A were found via the Levenberg−Marquardt

fitting routine in the Origin 8.5 software, whereas *n* was varied to obtain the best fit.[54] The calculated binding stoichiometry of the ligands with G-quadruplex telo21 was listed in Table S2 in supporting information.

2.6 Molecular docking study

Molecular docking study was performed using the solution structure of anti-parallel human telomeric DNA G-quadruplex (PDB ID: 2mb3) [55]. The first two thymine residues at the 5'-end and the last residue adenine at the 3'-end were deleted to produce 21-mer G-quadruplex. The NMR structure of duplex DNA 5'-d(CGCTAGCG)-3' in complex with homodimeric thiazole orange dye (TO) (PDB ID: 108D) was used for the modeling of intercalation interaction.[56] The 3D structures of the small molecules were generated with DS viewer 3.5. Autodock Tools (ver. 1.5.6) was used to convert the structure files to pdbqt format.[57] Docking was performed using the AUTODOCK vina program.[58] The dimensions of the active site box were chosen to be large enough to encompass the entire G-quadruplex structures. An exhaustiveness of 100 was used and other parameters were left as default.

2.7 Circular dichroism (CD) measurement

The concentration of telo21 was 5 μM in 10 mM Tris ‑ HCl, 60 mM KCl, pH = 7.4 and the concentration of the ligand was 1 to 3 folds in 5 mM Tris-HCl with 60 mM KCl at pH 7.4. The CD spectra were carried out using a Chirascan spectrophotometer (Applied Photophysics). The quartz cuvette with 4 mm path length was employed for the spectra recorded over a wavelength range of 230 to 450 nm at 1 nm bandwidth, 1 nm step size, and 0.5 s per point. The CD spectra were obtained by taking the average of at least three scans made from 230 to 450 nm at 25 °C. Final analysis of the data was carried out with Origin 7.5 (OriginLab Corp.).

2.8 FRET assay conditions

The FRET assay was performed as a high-throughput screen following previously published procedures.[44] The labeled oligonucleotides F21T: 5'-FAM-d(GGG[TTAGGG]3)-TAMRA-3' (donor fluorophore FAM is 6-carboxyfluorescein; acceptor fluorophore TAMRA is 6-carboxytetramethylrhodamine; HEG linker is $(–CH_2–CH_2–O–)_6$ used as the FRET probes were diluted from stock to the correct concentration (0.4 μM) in buffer and then annealed by heating to 95 °C for 5 min, followed by cooling to room temperature. Samples were prepared by aliquoting 15 μL of the annealed F21T (at 2 × concentration, 0.4 μM) into LightCycler 96, followed by 15 μL of the ligand

solution (at 2 × concentration, 0.2–2.0 μM) and further incubated for 1 h. Fluorescence melting curves were determined with a Roche LightCycler real-time PCR machine with excitation at 470 nm and detection at 530 nm. Fluorescence readings were taken at intervals of 3 °C over the temperature range of 37–93 °C, with a constant temperature being maintained for 300 s prior to each reading to ensure a stable value.

2.9 MTT experiment conditions

The cell lines at logarithmic growth stage were inoculated into two 96-well plates with a cell density of about 5000 cells per hole and then exposed to 37 °C and 5 % CO_2 respectively. After 48 h of inoculation, the medium was discarded, washed three times with PBS buffer, and then added to the medium containing different concentrations of gradient the compounds **1-3**. After incubation for 48 h, MTT (thiazole blue) solution (5 mg/mL) 20 μL was added into each hole (blank group without MTT coloration and control group without medicine). Continue incubation for 4 h at 37 C and 5% CO_2, the supernatant was discarded and DMSO 100 μL was added into each hole. After 15 s of oscillation, the chlamydia was fully dissolved. Finally, the absorbance of each hole at 492 nm was measured by enzyme labeling instrument, and the experimental results were recorded. The IC_{50} value of the compound can be obtained by mapping the cell viability.

3. Results and discussion

The fluorescent DNA binding ligands as shown in Scheme 1 were designed to bear a rotatable and π–conjugated substituent group at the 2-position of 1-methylquinolinium moiety of thiazole orange (TO). The ligands possess an extended π–conjugated molecular structure compared with thiazole orange. In the molecular design, the extended substituent groups including styrenyl, 2-vinylnaphthalenyl and 4-phenylbuta-1,3-dien-1-yl were designed systematically to increase the flexibility of the thiazole orange-based molecular scaffold as the substituent group was connected with thiazole orange via an ethylene bridge, which is more flexible than the methylene bridge in the parent thiazole orange scaffold. The resulting molecular structure of the new ligands is thus freely rotatable in solution. Moreover, three substituent groups have different size and length of bridge for the comparison study of binding site matching of G4-DNA. These factors may possibly contribute to the degree of fluorescent signal discrimination (G4-DNA versus duplex-DNA) in the *in vitro* ligand-DNA interaction. The compounds synthesized were purified with flash column chromatography and the isolated yields were found to be 79-85%. The compounds were characterized unambiguously with ^{1}H

and ^{13}C NMR and mass spectrometry before evaluated in the ligand-DNA interaction study and bioassays.

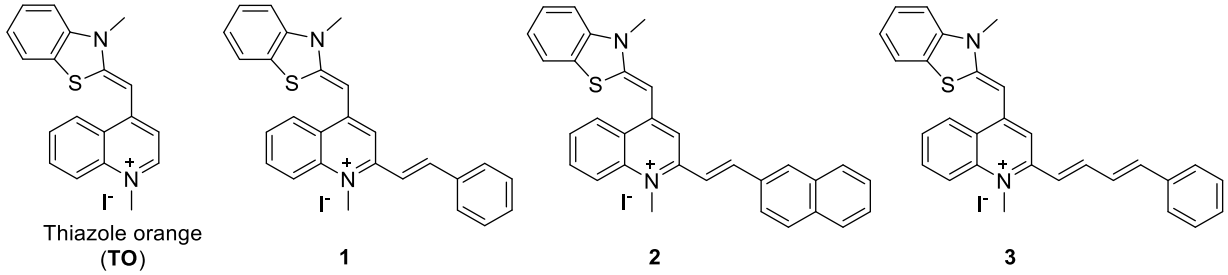

Scheme 1. The molecular structures of the fluorescent DNA binding ligands.

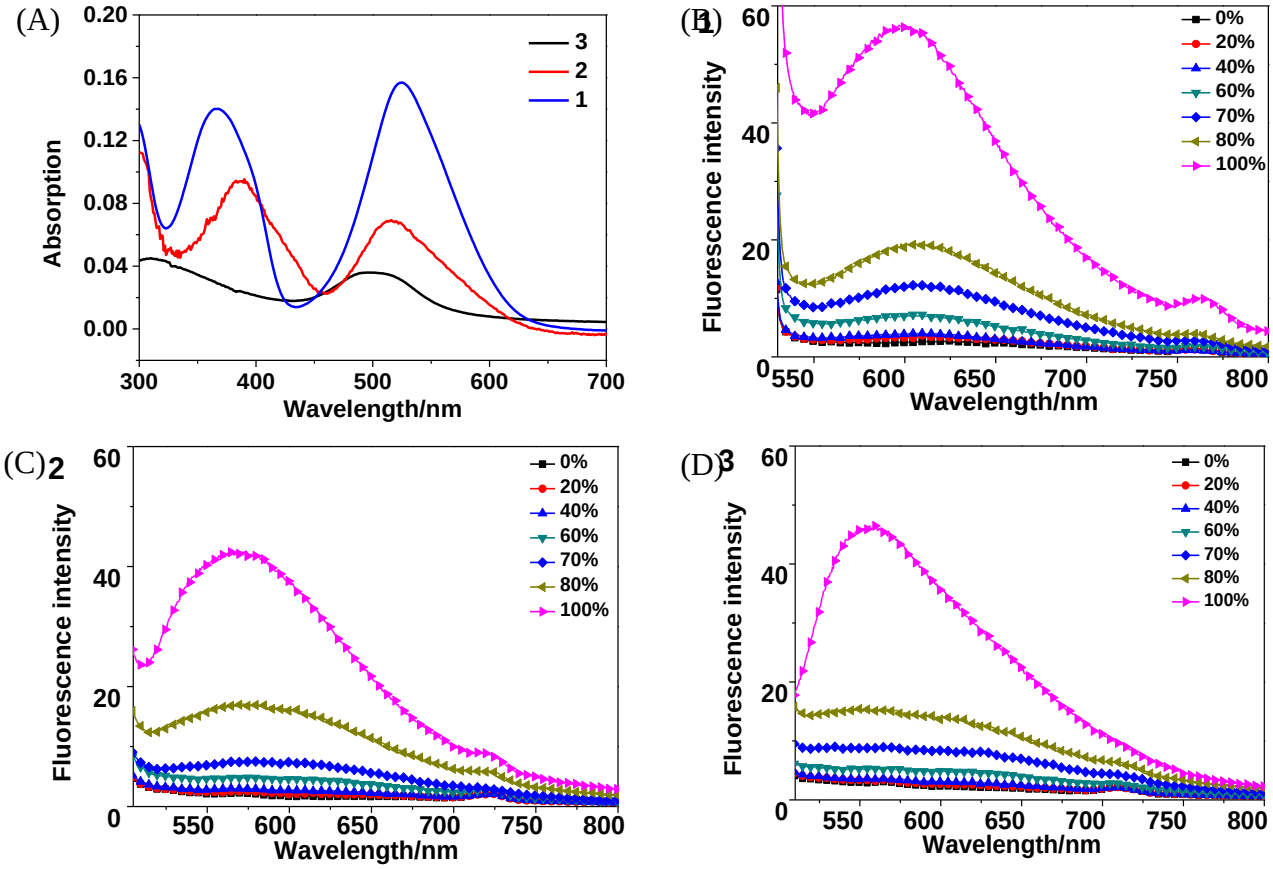

Figure 1. (A) The absorption spectra of ligands **1-3**; (B), (C) and (D) showed the fluorescent signal changes of ligands in the medium with different viscosity (glycerol/water, v/v %).

The UV-vis absorption of the compounds **1-3** were measured in a Tris-HCl buffer solution (pH 7.4). The major absorption peak (λ_{max}) observed in the long wavelength region was in the range of 499-525 nm as shown in Figure 1 (A). The ligands dissolved in the buffer solution display almost no background fluorescence because the molecular fragments of benzothiazole and the substituent group are freely rotatable and therefore cause radiationless decays when the ligand is in excited electronic states. However, when these rotations are restricted, it results the termination of the non-radiative decay channel and the fluorescence of the ligands that possess a π–conjugated aromatic system is restored.[59] The fluorescence feature of the new ligands is therefore sensitive to the rigidity of the environment. To demonstrate this fluorescence property, the ligands were dissolved in aqueous medium mixed with glycerol (v/v %). The water-glycerol ratio was adjusted to regulate the viscosity of the medium. The changes of fluorescence intensity of the ligands with excitation wavelength (λ_{ex}) at 510 nm were measured in the medium. As shown in Figure 1 B-D, the ligands in water medium showed very low background emission signal. However, the fluorescence intensity was increased gradually as increasing the content of glycerol in the medium, which indicated the increasing of viscosity of the medium. Moreover, the fluorescence intensity reached maximum in 100 % glycerol because of its high viscosity. The results may support that the fluorescence property of the ligand is sensitive to rigidity of the environment and the restoration of fluorescence may be mainly due to the significant restricted molecular rotation is in the highly viscous glycerol medium.[60] This implies that when the ligands interact with G4-DNA with significant binding affinity, it may be able to suppress the radiationless decays because the ligand-DNA interaction may induce high barrier for the intramolecular torsional motion, resulting fluorescence signal regarding to the interaction, which is important for both *in vitro* or *in vivo* molecular recognition and sensing.

The fluorescence change and binding affinity of the ligands were investigated with a series of DNA substrates in Tris-HCl buffer solution under room temperature conditions. In the fluorescence assays, two single-stranded DNAs (dt21, da21), four double-stranded DNAs (4a4t, 4at, ds12, ds26), and thirteen G4-DNAs (telomere DNA: htg22, telo21, 4telo, human12, oxy12, oxy28; promoter DNA: pu27, bc12, pu18, VEGF, RET, cik-1, ckit-2) were studied. Ligands **1-3** treated independently with these DNA substrates were excited (λ_{ex} = 510 nm) and their enhanced fluorescence signals were measured for the comparison of interaction selectivity. From Figure 2, it was found that different degree of fluorescence signals were observed upon the ligand bound with different DNA substrates, which may indicate that the ligands exhibit certain recognition selectivity. The enhanced fluorescence signal intensity revealed the *in-situ* ligand-DNA interactions [61, 62] and this induced signal is an

indicator for the target specificity. With respect to the fluorescence screening results, it is generally observed that the telomeric G4-DNA substrates gave much higher induced fluorescence signal than the double-stranded DNA (dsDNA) while the promoter G4-DNA was just slightly better than dsDNA. Moreover, the single-stranded DNA (ssDNA) substrates were only induced very weak fluorescence signal upon bound with the ligands. It is noteworthy that ligand **1** displayed the best performance in the recognition selectivity for telomeric G4-DNA versus dsDNA because the induced interaction signal of **1** with telomeric G4-DNA is at least 2-fold higher than that of dsDNA (Figure 2).

To further understand the discrimination ability of the ligands towards different types of DNA, the representative substrates were selected for comparison in the fluorescence titrations. The typical nucleic acid substrates including telo21 (G4-DNA), ds26 (double-stranded DNA), da21 (single-stranded DNA) and RNA were investigated for their interactions with the ligands. From the titration experiments, the interaction signals were observed (F/F_0) and the ligands generally have a higher binding selectivity towards telo21 than ds26, while both ssDNA and RNA exhibited much weaker interaction signal (Figure 3). Previous study demonstrated that thiazole orange showed no significant fluorescent discrimination ability between telomeric G4-DNA and dsDNA.[37] This suggested that the observed binding selectivity for the ligands with various DNA substrates could be possibly attributed to the introduced substituent of the thiazole orange scaffold. We speculated that whether the whole molecule could be located inside the G4-binding pocket may be one of the critical factors to induce fluorescent discrimination ability because the structural environment of the G4-DNA binding site (G-quartet) is relatively rigid. Considering that if the molecular scaffold of the ligand with a suitable sized substituent group, it could be well matched for end-stacking onto the planar surface of G-quartet and may also establish a good binding affinity to achieve better fluorescent discrimination ability against other type of nucleic acids.

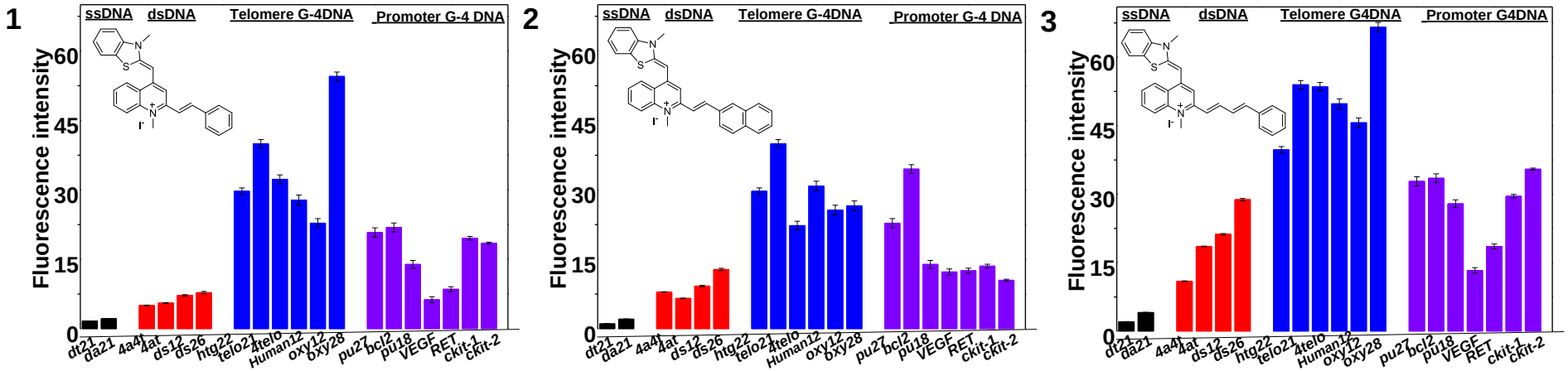

Figure 2. Comparison of DNA selectivity of ligands towards different nucleic acids in a Tris-HCl buffer solution containing 60 mM KCl. The final concentration of ligand was at 5 μM and DNA concentration used was 10 μM. The excitation wavelength (λ_{ex}) was 510 nm and the fluorescence signal (λ_{em}) was recorded at emission maxima: **1**, λ_{em} = 620 nm; **2**, λ_{em} = 530 nm and **3**, λ_{em} = 550 nm. The interaction signals were measured after incubation for 10 min at 25 °C.

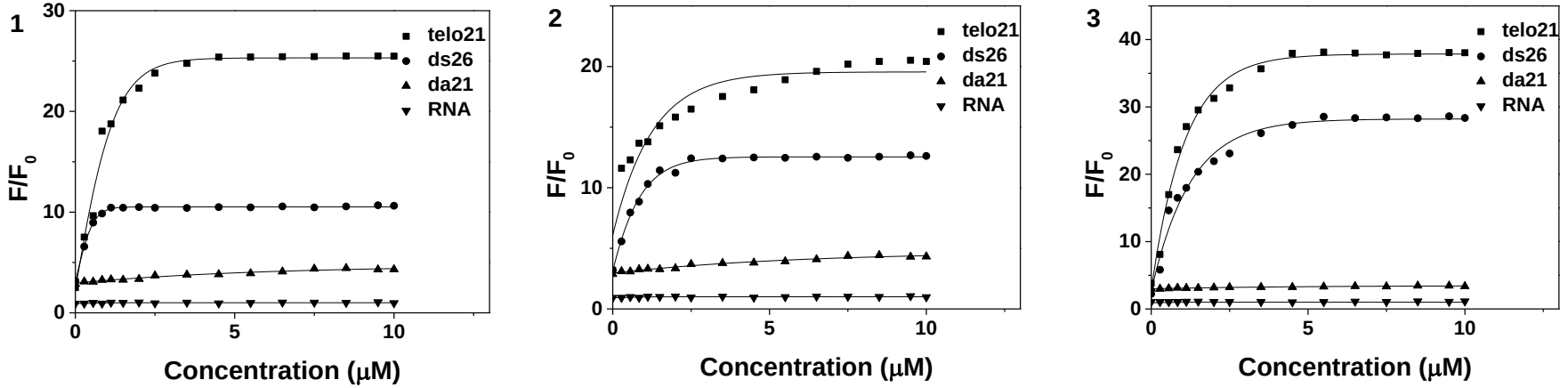

Figure 3. The equilibrium binding study of ligands with representative nucleic acids (ssDNA: da21, dsDNA: ds26, G4-DNA: telo21, and RNA) at various concentrations. In the fluorescence titrations, the excitation wavelength was λ_{ex} = 510 nm and the fluorescence signal (λ_{em}) was recorded at emission maxima of ligands: **1**, λ_{em} = 620 nm; **2**, λ_{em} = 530 nm and **3**, λ_{em} = 550 nm. The final concentration of ligand was fixed at 5 μM in a Tris–HCl buffer containing 60 mM KCl. Measurements were taken after incubated for 10 min at 25 °C.

Table 1. Comparison of quantum yields of the ligand-DNA complex formed *in vitro* and their equilibrium binding constants.[a]

Ligand	$\varepsilon_{510\ nm,}$ [b] $M^{-1}cm^{-1}$	Emission λ_{em} (nm)	Quantum yield, Φ_f [c]	K_{telo21} ($x10^5\ M^{-1}$) [d]	K_{ds26} ($x10^5\ M^{-1}$) [c]	K_{telo21} / K_{ds26}
1	27400	620	0.051	1.05±0.09	0.24±0.07	4.4
2	13500	530	0.054	0.89±0.14	0.32±0.05	2.7
3	7030	550	0.021	1.44±0.21	0.78±0.11	1.8

[a] Experiments were performed in 10 mM Tris-HCl buffer at pH 7.4 at 25 °C.

[b] Molar extinction coefficient (ε) at 510 nm.

[c] Relative fluorescence quantum yield of ligand upon addition of 3 μM telo21. The standard used for the determination of relative fluorescence quantum yields was fluorescein (Φ_f = 0.85, in 0.1 N $NaOH_{(aq)}$).[51]

[d] Equilibrium binding constant (K_{telo21}) between the ligand and telo21 G4-DNA.

[e] Equilibrium binding constant (K_{ds26}) between the ligand and double-stranded DNA ds26.

From the titration experiments shown in Figure 3, the ligands upon bound to telo21 or ds26 induced significant fluorescence signals, indicating the *in-situ* formation of ligand-DNA complex. The quantum yields of the ligand-telo21 complexes were found in the range of 0.021-0.054. In addition, the equilibrium binding constants of the ligands interacting with telo21 and ds26 were estimated. However, for substrates da21 and RNA, their fluorescence interaction signals were found too weak for estimating equilibrium binding constants with reasonable accuracy. From Table 1, the K_{telo21} values were found in the range of 0.89 – 1.44 x $10^5\ M^{-1}$, which is generally higher than that of K_{ds26} (0.24 – 0.78 x $10^5\ M^{-1}$). By comparing the equilibrium binding constants, it may suggest that the ligands exhibit higher binding affinity and selectivity towards G4-DNA over duplex DNA. Moreover, as indicated from K_{telo21}/K_{ds26} ratio = 4.4, ligand **1** showed the better binding selectivity for G4-DNA against dsDNA. Among the ligands sharing the same thiazole orange core scaffold but bearing different substituent groups, ligand **1** has the smallest molecular size that may lead to better binding selectivity towards G4-DNA over dsDNA. This could be probably due to its molecular size matched well with the rigid G4-DNA binding pocket. To get better understanding on this speculation, molecular docking study was thus performed to compare the possible mode of ligand binding with the G-quartet.

The molecular docking results of the three ligands in complex with telo21 G4-DNA and ds26 duplex DNA were shown in Figure 4. The three ligands are able to stack on the telo21 G-quartet in a

very similar way as our previous report [37], while subtle differences can be found. Ligand **1** is well-matched with the G-quartet and is completely embedded in the G-quartet binding pocket (Figure 4 A), suggesting a good binding affinity and fluorescent property upon interaction. It seems that the size of **2** with a naphthalene substituent is slightly bigger than the G-quartet, while a strong stacking interaction can still be visualized with two major pharmacophores (TO and napthalene) (Figure 4 B). However, it is observed that the oversized **3** along with its flexible diene linkage would result less matched in the binding site of G-quartet. The homodimeric TO is known to intercalate in the ds26 duplex DNA with the 5'-CpT-3' binding site being stacked by TO chromophore [56]. In the present study, all three ligands intercalate in the 5'-CpT-3' binding site in the same way and orientation with their substituent groups at the 2-position of TO pointing out of the binding site (Figure 4 D, E, F). The substituent groups outside the binding pocket are likely to interact with solvent and thus lead to negative effects on both binding affinity and fluorescence signal [63]. The ligands may be more loosely bound with duplex DNA as compared to the situation when bound with G-quadruplex. These docking results indicate that the three ligands have selectivity towards G4-DNA over dsDNA.

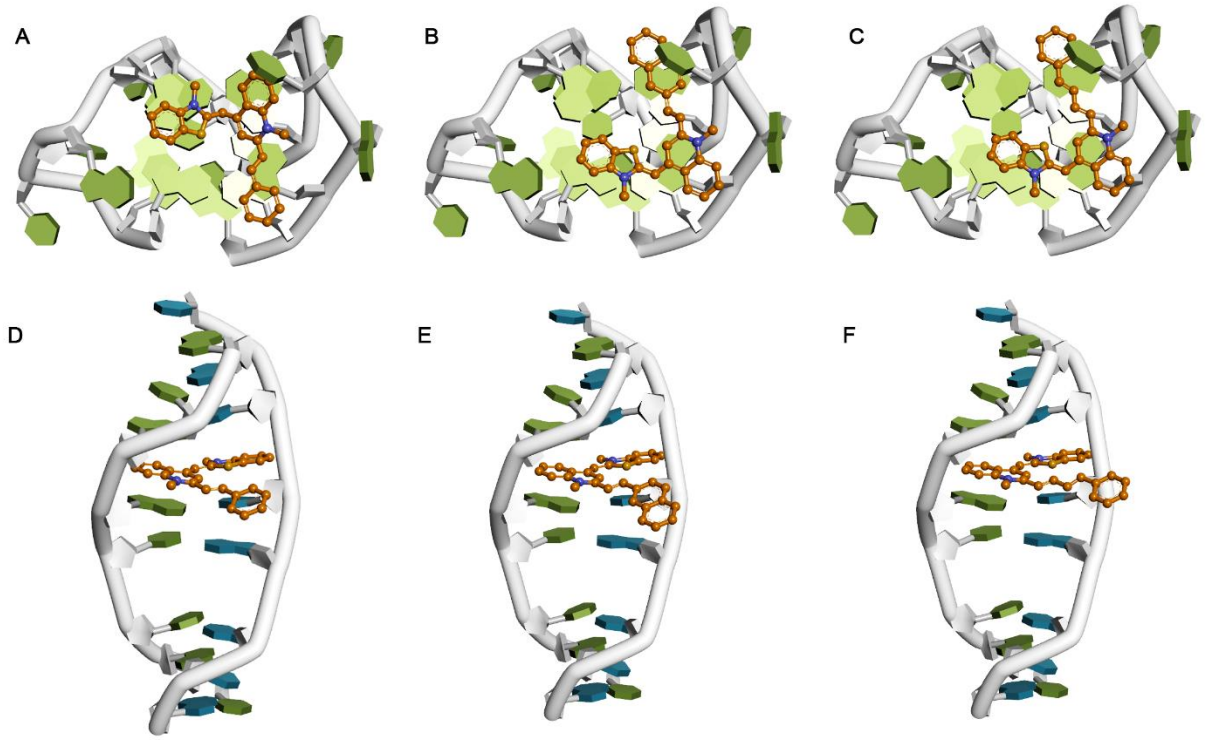

Figure 4. (A, B, C) The binding mode of the ligands (**1, 2 and 3**) with telo21 G4-DNA (PDB ID: 2mb3) and (D, E, F) ds26 duplex DNA (PDB ID: 108D).

To understand the possible G4-structure conformation influence caused by the ligand upon binding, circular dichroism (CD) spectroscopy was utilized to investigate the interaction between ligand **1** and telo21. From the CD spectra shown in Figure 5 A, with telo21 alone, it shows that a small positive absorption peak at 245 nm, a major negative absorption peak at 261 nm and a major positive and broad absorption peak at 292 nm. These characteristic absorption patterns may indicate that the anti-parallel type of topology of telo21 was formed mainly in the buffered solution with K^+ ions. Moreover, a pair of very weak absorption peaks found at 235 nm (native peak) and 269 nm (positive peak) may reveal the presence of parallel G4-structure.[63] Therefore, both parallel and anti-parallel types of topology may co-exist in the buffered solution while the anti-parallel G4-structure is more favorable. With the addition of **1** to bind to telo21, the absorption peak at 269 nm was influenced and became smaller while the peak at 261 nm became more negative. The CD results may indicate that the anti-parallel G4-structure has no significant influence upon binding to the ligand whereas the parallel G4 could possibly change to anti-parallel in order to adopt a more stable complex in solution.

In addition, fluorescence-based (FRET) melting assays were performed to evaluate the stabilization ability of ligands **1-3** for G4-structure. The normalized FRET melting curves of G4-DNA F21T at different concentration of ligands were shown in Figure S5. With the addition of the ligands at 2 μM, the ΔT_m values shown in Figure 5 B were increased in the range of 3.3-11.2 °C generally. The control experiments using F10T (duplex DNA) showed that the ΔT_m values obtained were slightly increased from 1.1-1.6 °C under the same conditions, which are significantly less than that of G4-DNA F21T. The results of FRET melting assays may suggest that the binding ligands, particularly **1** and **2**, could stabilize G4-structure better than double-stranded DNA.[63]

Taking together all the results obtained from equilibrium binding constants, increased ΔT_m values and molecular docking study, it may suggest that the ligands generally exhibit a favorable interaction with G4-structure over duplex DNA *in vitro*. We therefore investigated their cytotoxicity against cancer cells and evaluated the potential of these molecular scaffolds in anticancer application and drug design. MTT assays were performed to evaluate the cytotoxicity of the ligands in two selected cancer cell lines (human prostate cancer cell (PC3) and human hepatoma cell (hepG2). The inhibitory effects on cell growth were shown in Table 2. The IC_{50} values obtained were in the range of 6.3–12.5 μM, which may indicate that the ligands display relatively high cytotoxicity towards both PC3 and hepG2 cells. The inhibitory mechanism of the ligands is not clear at this stage but the cytotoxicity observed against the cancer cells could be potentially attributed to the *in vivo* DNA-ligand interactions, such as binding to the DNA G-quadruplexes and/or double-stranded DNA, and thus interrupting the cell

growth.[64] However, a more in-depth investigation is necessary in order to understand better the underlying mechanism.

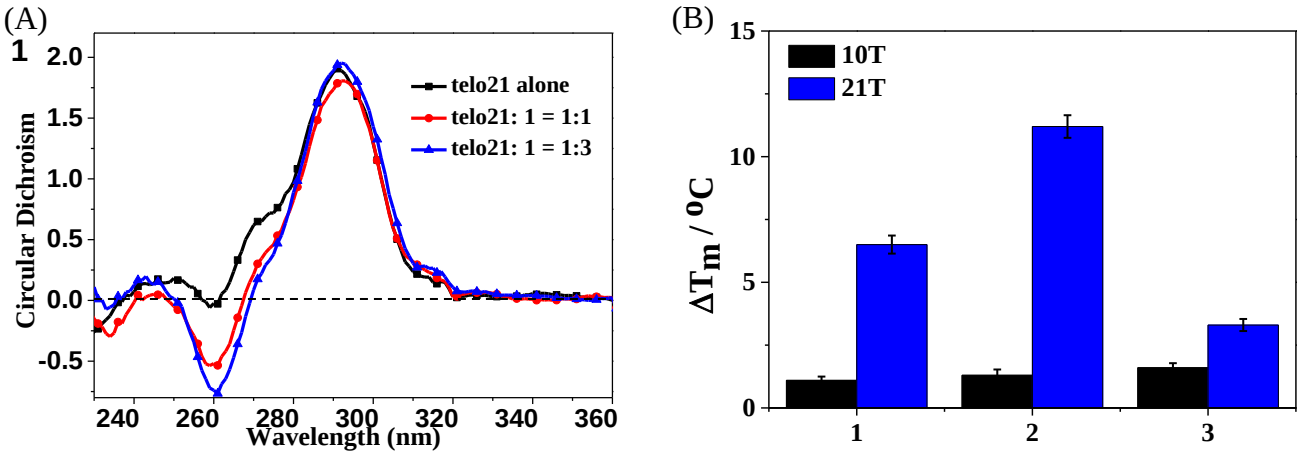

Figure 5. (A) The CD spectra of the DNA binding ligand **1** bound to telo21 (5 μM) in a buffered solution of 10 mM Tris–HCl and 60 mM KCl at pH = 7.4; (B) The stabilization of telomere G-quadruplex DNA structure with the ligands in FRET-melting assays.

Table 2. Evaluation of cytotoxicity (IC_{50}) the DNA binding ligands against cancer cells with MTT assays.[a]

Ligand	IC_{50}, μM	
	PC3	HepG2
1	9.8	6.3
2	12.4	8.8
3	12.5	9.4

[a] Inhibition rate (%) = (Control group average OD - Experimental group average OD)/Control group average OD x 100%. $lgIC_{50} = X_m\text{-}I\ (P\text{-}(3\text{-}P_m\text{-}P_n)/4)$. Where X_m: lg(maximum dose); I: lg(maximum dose/adjacent dose); P is the sum of positive response rates; P_m is the largest positive response rate; P_n is the smallest positive response rate.

Conclusion

In conclusion, three new fluorescent DNA binding ligands were synthesized by the introduction of a small and conjugated group at the 2-position of the 1-methylquinolinium moiety of thiazole orange. The ligands were investigated in fluorescence binding assays and showed significant recognition selectivity towards G4-DNA over duplex-DNA, which is found in accord with the results obtained from the equilibrium binding study, the G4-DNA stabilization ability study with FRET melting assays and molecular docking. Among the ligands, the molecular structure of **1** showed better binding site

matching with the G-quartet. In addition, the cytotoxicity (IC_{50}) of these fluorescent DNA binding ligands evaluated in MTT assays against the cancer cell lines of human prostate cancer cell (PC3) and human hepatoma cell (hepG2) was found in the range of 6.3–12.5 μM, which indicated that the ligands may have relatively high cytotoxicity towards the tested cancer cells.

Acknowledgement

The project is supported by the Natural Science Foundation of Guangdong Province, China (Grant No.: 2019A1515011799) and Jiangmen Program for Innovative Research Team (No. 2018630100180019806). We also acknowledge the supports received from the State Key Laboratory of Chemical Biology and Drug Discovery, Department of Applied Biology and Chemical Technology, The Hong Kong Polytechnic University.

Reference

[1] J.D. Watson, F.H. Crick, Genetical implications of the structure of deoxyribonucleic acid, Nature, 171 (1953) 964-967.
[2] M. Kaushik, S. Kaushik, K. Roy, A. Singh, S. Mahendru, M. Kumar, S. Chaudhary, S. Ahmed, S. Kukreti, A bouquet of DNA structures: Emerging diversity, Biochem. Biophys. Rep., 5 (2016) 388-395.
[3] A. Bacolla, D.N. Cooper, K.M. Vasquez, DNA structure matters, Genome Med., 5 (2013) 51.
[4] M. Kaushik, A. Bansal, S. Saxena, S. Kukreti, Possibility of an antiparallel (tetramer) quadruplex exhibited by the double repeat of the human telomere, Biochem., 46 (2007) 7119-7131.
[5] A. Siddiqui-Jain, C.L. Grand, D.J. Bearss, L.H. Hurley, Direct evidence for a G-quadruplex in a promoter region and its targeting with a small molecule to repress c-MYC transcription, Proc. Natl. Acad. Sci. U.S.A., 99 (2002) 11593-11598.
[6] D. Varshney, J. Spiegel, K. Zyner, D. Tannahill, S. Balasubramanian, The regulation and functions of DNA and RNA G-quadruplexes, Nat. Rev. Mol. Cell Biol., (2020) 1-16.
[7] T. Tian, Y.-Q. Chen, S.-R. Wang, X. Zhou, G-Quadruplex: a regulator of gene expression and its chemical targeting, Chem, 4 (2018) 1314-1344.
[8] B. Onel, M. Carver, G. Wu, D. Timonina, S. Kalarn, M. Larriva, D. Yang, A new G-quadruplex with hairpin loop immediately upstream of the human BCL2 P1 promoter modulates transcription, J. Am. Chem. Soc., 138 (2016) 2563-2570.
[9] R.M. Brosh Jr, DNA helicases involved in DNA repair and their roles in cancer, Nat. Rev. Cancer, 13 (2013) 542-558.
[10] M.-Y. Kim, H. Vankayalapati, K. Shin-Ya, K. Wierzba, L.H. Hurley, Telomestatin, a potent telomerase inhibitor that interacts quite specifically with the human telomeric intramolecular G-quadruplex, J. Am. Chem. Soc., 124 (2002) 2098-2099.
[11] M.-H. Hu, S.-B. Chen, B. Wang, T.-M. Ou, L.-Q. Gu, J.-H. Tan, Z.-S. Huang, Specific targeting of telomeric multimeric G-quadruplexes by a new triaryl-substituted imidazole, Nucleic Acids Res., 45 (2017) 1606-1618.
[12] J. Spiegel, S. Adhikari, S. Balasubramanian, The structure and function of DNA G-quadruplexes, Trends Chem., 2 (2020) 123-136.

[13] S.L. König, A.C. Evans, J.L. Huppert, Seven essential questions on G-quadruplexes, Biomol. concepts, 1 (2010) 197-213.
[14] J.F. Moruno-Manchon, P. Lejault, Y. Wang, B. McCauley, P. Honarpisheh, D.A.M. Scheihing, S. Singh, W. Dang, N. Kim, A. Urayama, Small-molecule G-quadruplex stabilizers reveal a novel pathway of autophagy regulation in neurons, Elife, 9 (2020) e52283.
[15] A.K. Todd, M. Johnston, S. Neidle, Highly prevalent putative quadruplex sequence motifs in human DNA, Nucleic Acids Res., 33 (2005) 2901-2907.
[16] J.L. Huppert, S. Balasubramanian, Prevalence of quadruplexes in the human genome, Nucleic Acids Res., 33 (2005) 2908-2916.
[17] L.Y. Liu, W. Liu, K.N. Wang, B.C. Zhu, X.Y. Xia, L.N. Ji, Z.W. Mao, Quantitative Detection of G-Quadruplex DNA in Live Cells Based on Photon Counts and Complex Structure Discrimination, Angew. Chem. Int. Ed., (2020).
[18] R. Kumar, K. Chand, S. Bhowmik, R.N. Das, S. Bhattacharjee, M. Hedenström, E. Chorell, Subtle structural alterations in G-quadruplex DNA regulate site specificity of fluorescence light-up probes, Nucleic Acids Res., (2020).
[19] P.A. Summers, B. Lewis, J. Gonzalez-Garcia, A.H. Lim, P. Cadinu, R.M. Porreca, N. Martin-Pintado, D. Mann, J.B. Edel, J.-B. Vannier, Visualising G-quadruplex DNA dynamics in live cells by fluorescence lifetime imaging microscopy, bioRxiv, (2020).
[20] M.I. Umar, D. Ji, C.-Y. Chan, C.K. Kwok, G-Quadruplex-Based Fluorescent Turn-On Ligands and Aptamers: From Development to Applications, Molecules, 24 (2019) 2416.
[21] F. Gao, S. Cao, W. Sun, S. Long, J. Fan, X. Peng, Development of a two-photon carbazole derivative probe for fluorescent visualization of G-quadruplex DNA in cells, Dyes Pigm., 171 (2019) 107749.
[22] C. Kotras, M. Fossépré, M. Roger, V. Gervais, S. Richeter, P. Gerbier, S. Ulrich, M. Surin, S. Clément, A cationic tetraphenylethene as a light-up supramolecular probe for DNA G-quadruplexes, Front. Chem., 7 (2019) 493.
[23] D. Monchaud, Quadruplex detection in human cells, arXiv preprint arXiv:1910.07023, (2019).
[24] S. Zhang, H. Sun, L. Wang, Y. Liu, H. Chen, Q. Li, A. Guan, M. Liu, Y. Tang, Real-time monitoring of DNA G-quadruplexes in living cells with a small-molecule fluorescent probe, Nucleic Acids Res., 46 (2018) 7522-7532.
[25] A. Laguerre, J.M. Wong, D. Monchaud, Direct visualization of both DNA and RNA quadruplexes in human cells via an uncommon spectroscopic method, Sci. Rep., 6 (2016) 32141.
[26] A. Shivalingam, M.A. Izquierdo, A. Le Marois, A. Vyšniauskas, K. Suhling, M.K. Kuimova, R. Vilar, The interactions between a small molecule and G-quadruplexes are visualized by fluorescence lifetime imaging microscopy, Nat. Commun., 6 (2015) 1-10.
[27] G. Biffi, D. Tannahill, J. McCafferty, S. Balasubramanian, Quantitative visualization of DNA G-quadruplex structures in human cells, Nat. Chem., 5 (2013) 182.
[28] R. Rodriguez, K.M. Miller, J.V. Forment, C.R. Bradshaw, M. Nikan, S. Britton, T. Oelschlaegel, B. Xhemalce, S. Balasubramanian, S.P. Jackson, Small-molecule–induced DNA damage identifies alternative DNA structures in human genes, Nat. Chem. Biol., 8 (2012) 301.
[29] V. Dhamodharan, P.I. Pradeepkumar, Specific Recognition of Promoter G-Quadruplex DNAs by Small Molecule Ligands and Light-up Probes, ACS Chem. Biol., 14 (2019) 2102-2114.
[30] A. Renaud de la Faverie, A. Guedin, A. Bedrat, L.A. Yatsunyk, J.-L. Mergny, Thioflavin T as a fluorescence light-up probe for G4 formation, Nucleic Acids Res., 42 (2014) e65-e65.

[31] F. Doria, A. Oppi, F. Manoli, S. Botti, N. Kandoth, V. Grande, I. Manet, M. Freccero, A naphthalene diimide dyad for fluorescence switch-on detection of G-quadruplexes, Chem. Commun., 51 (2015) 9105-9108.
[32] M.-Q. Wang, S. Liu, C.-P. Tang, A. Raza, S. Li, L.-X. Gao, J. Sun, S.-P. Guo, Flexible amine-functionalized triphenylamine derivative as a fluorescent "light-up" probe for G-quadruplex DNA, Dyes Pigm., 136 (2017) 78-84.
[33] I. Czerwinska, B. Juskowiak, Photoisomerizable arylstilbazolium ligands recognize parallel and antiparallel structures of G-quadruplexes, Int. J. Biol. Macromol., 51 (2012) 576-582.
[34] Y.-J. Lu, X.-L. Guo, M.-H. Xu, W.-W. Chen, W.-L. Wong, K. Zhang, C.-F. Chow, Selective visualization of DNA G-quadruplex structures in live cells with 1-methylquinolinium-based molecular probes: The importance of indolyl moiety position towards specificity, Dyes Pigm., 143 (2017) 331-341.
[35] B.-X. Zheng, W. Long, Y.-H. Zhang, X.-H. Huang, C.-C. Chen, D.-X. Zhong, M.-T. She, Z.-X. Chen, D.-P. Cai, Y.-J. Lu, Rational design of red fluorescent and selective G-quadruplex DNA sensing probes: The study of interaction signaling and the molecular structural relationship achieving high specificity, Sens. Actuators, B, (2020) 128075.
[36] L. Zhang, X. Liu, S. Lu, J. Liu, S. Zhong, Y. Wei, T. Bing, N. Zhang, D. Shangguan, Thiazole Orange Styryl Derivatives as Fluorescent Probes for G-Quadruplex DNA, ACS Appl. Bio. Mater., (2020).
[37] Y.-J. Lu, Q. Deng, J.-Q. Hou, D.-P. Hu, Z.-Y. Wang, K. Zhang, L.G. Luyt, W.-L. Wong, C.-F. Chow, Molecular engineering of thiazole orange dye: Change of fluorescent signaling from universal to specific upon binding with nucleic acids in bioassay, ACS Chem. Biol., 11 (2016) 1019-1029.
[38] X. Fei, Y. Gu, Y. Lan, B. Shi, Fluorescent properties of novel dendrimer dyes based on thiazole orange, J. Lumin., 131 (2011) 2148-2152.
[39] T.-Y. Tseng, W.-W. Chen, I.-T. Chu, C.-L. Wang, C.-C. Chang, M.-C. Lin, P.-J. Lou, T.-C. Chang, The G-quadruplex fluorescent probe 3, 6-bis (1-methyl-2-vinyl-pyridinium) carbazole diiodide as a biosensor for human cancers, Sci. Rep., 8 (2018) 1-7.
[40] N.C. Sabharwal, V. Savikhin, J.R. Turek-Herman, J.M. Nicoludis, V.A. Szalai, L.A. Yatsunyk, N-methylmesoporphyrin IX fluorescence as a reporter of strand orientation in guanine quadruplexes, FEBS J., 281 (2014) 1726-1737.
[41] J.-H. Guo, L.-N. Zhu, D.-M. Kong, H.-X. Shen, Triphenylmethane dyes as fluorescent probes for G-quadruplex recognition, Talanta, 80 (2009) 607-613.
[42] L. Martino, A. Virno, B. Pagano, A. Virgilio, S. Di Micco, A. Galeone, C. Giancola, G. Bifulco, L. Mayol, A. Randazzo, Structural and thermodynamic studies of the interaction of distamycin A with the parallel quadruplex structure [d (TGGGGT)] 4, J. Am. Chem. Soc., 129 (2007) 16048-16056.
[43] M. Arévalo-Ruiz, S. Amrane, F. Rosu, E. Belmonte-Reche, P. Peñalver, J.-L. Mergny, J.C. Morales, Symmetric and dissymmetric carbohydrate-phenyl ditriazole derivatives as DNA G-quadruplex ligands: Synthesis, biophysical studies and antiproliferative activity, Bioorg. Chem., (2020) 103786.
[44] Y.-J. Lu, D.-P. Hu, K. Zhang, W.-L. Wong, C.-F. Chow, New pyridinium-based fluorescent dyes: A comparison of symmetry and side-group effects on G-Quadruplex DNA binding selectivity and application in live cell imaging, Biosens. Bioelectron., 81 (2016) 373-381.
[45] J. Jin, J. Hou, W. Long, X. Zhang, Y.-J. Lu, D. Li, K. Zhang, W.-L. Wong, Synthesis of fluorescent G-quadruplex DNA binding ligands for the comparison of terminal group effects in molecular interaction: phenol versus methoxybenzene, Bioorg. Chem., (2020) 103821.

[46] D. Li, J.-Q. Hou, W. Long, Y.-J. Lu, W.-L. Wong, K. Zhang, A study on a telo21 G-quadruplex DNA specific binding ligand: enhancing the molecular recognition ability via the amino group interactions, RSC Adv., 8 (2018) 20222-20227.
[47] M. O'Hagan, P. Peñalver, R. Fisher, J.C. Morales, M.C. Galan, Stiff-Stilbene Ligands Target G-Quadruplex DNA and Exhibit Selective Anticancer and Antiparasitic Activity, Chem. Eur. J., (2020).
[48] M.-Q. Wang, X.-N. Liu, Z.-J. Guo, C. Feng, M. Rui, Synthesis of quinolinium-based probes and studies of their effects for selective G-quadruplex DNA targeting, New J. Chem., 42 (2018) 4933-4939.
[49] D. Li, W. Long, J. Hou, Q. Deng, Q. Guo, W.-L. Wong, Y.-J. Lu, K. Zhang, A series of modified thiazole orange dye as the highly fluorescent G-quadruplex DNA binders: The study of electronic effects of the substituent on 1-methylquinolinium moiety, J. Lumin., 205 (2019) 367-373.
[50] C. Ehrt, T. Brinkjost, O. Koch, Impact of binding site comparisons on medicinal chemistry and rational molecular design, J. Med. Chem., 59 (2016) 4121-4151.
[51] C.A. Parker, W. Rees, Correction of fluorescence spectra and measurement of fluorescence quantum efficiency, Analyst, 85 (1960) 587-600.
[52] H.J. Yvon, A guide to recording fluorescence quantum yields, HORIBA Jobin Yvon Inc, Stanmore, Middlesex, UK, (2012).
[53] F.H. Stootman, D.M. Fisher, A. Rodger, J.R. Aldrich-Wright, Improved curve fitting procedures to determine equilibrium binding constants, Analyst, 131 (2006) 1145-1151.
[54] X. Xie, B. Choi, E. Largy, R. Guillot, A. Granzhan, M.P. Teulade-Fichou, Asymmetric distyrylpyridinium dyes as red-emitting fluorescent probes for quadruplex DNA, Chem. Eur. J., 19 (2013) 1214-1226.
[55] W.J. Chung, B. Heddi, M. Tera, K. Iida, K. Nagasawa, A.T. Phan, Solution structure of an intramolecular (3+ 1) human telomeric G-quadruplex bound to a telomestatin derivative, J. Am. Chem. Soc., 135 (2013) 13495-13501.
[56] H.P. Spielmann, D.E. Wemmer, J.P. Jacobsen, Solution structure of a DNA complex with the fluorescent bis-intercalator TOTO determined by NMR spectroscopy, Biochem., 34 (1995) 8542-8553.
[57] G.M. Morris, R. Huey, W. Lindstrom, M.F. Sanner, R.K. Belew, D.S. Goodsell, A.J. Olson, AutoDock4 and AutoDockTools4: Automated docking with selective receptor flexibility, J. Comput. Chem. , 30 (2009) 2785-2791.
[58] S. Forli, R. Huey, M.E. Pique, M.F. Sanner, D.S. Goodsell, A.J. Olson, Computational protein–ligand docking and virtual drug screening with the AutoDock suite, Nat. Protoc., 11 (2016) 905.
[59] G.L. Silva, V. Ediz, D. Yaron, B.A. Armitage, Experimental and computational investigation of unsymmetrical cyanine dyes: understanding torsionally responsive fluorogenic dyes, J. Am. Chem. Soc., 129 (2007) 5710-5718.
[60] V.R. Mishra, C.W. Ghanavatkar, N. Sekar, ESIPT clubbed azo dyes as deep red emitting fluorescent molecular rotors: Photophysical properties, pH study, viscosity sensitivity, and DFT studies, J. Lumin., 215 (2019) 116689.
[61] F.-Y. Wu, Y.-L. Xiang, Y.-M. Wu, F.-Y. Xie, Study of interaction of a fluorescent probe with DNA, J. Lumin., 129 (2009) 1286-1291.
[62] A. Rožman, I. Crnolatac, T. Deligeorgiev, I. Piantanida, Strong impact of chloro substituent on TOTO and YOYO ds-DNA/RNA sensing, J. Lumin., 205 (2019) 87-96.
[63] A. De Rache, J.-L. Mergny, Assessment of selectivity of G-quadruplex ligands via an optimised FRET melting assay, Biochimie, 115 (2015) 194-202.

[64] J. Riou, L. Guittat, P. Mailliet, A. Laoui, E. Renou, O. Petitgenet, F. Megnin-Chanet, C. Helene, J. Mergny, Cell senescence and telomere shortening induced by a new series of specific G-quadruplex DNA ligands, Proc. Natl. Acad. Sci. U.S.A., 99 (2002) 2672-2677.

Supporting information

Structural modification of nonspecific thiazole orange for ligand-DNA interaction study: Understanding the ligand recognition selectivity towards G4-DNA over duplex-DNA

Yiwen Zhu [a,‡], Jinqiang Hou [d,‡], Xuan-He Huang [c], Dong-Xiao Zhong [c], Wei Long [c], Wenjie Liu [d], Yu-Jing Lu [c], Kun Zhang [e], and Wing-Leung Wong [b,e,*]

[a] College of Materials and Environmental Engineering, Hangzhou Dianzi University, Hangzhou, 310018, P. R. China.

[b] The State Key Laboratory of Chemical Biology and Drug Discovery, Department of Applied Biology and Chemical Technology, The Hong Kong Polytechnic University, Hung Hom, Kowloon, Hong Kong, China.

[c] Institute of Natural Medicine and Green Chemistry, School of Chemical Engineering and Light Industry, Guangdong University of Technology, Guangzhou 510006, P. R. China.

[d] Department of Chemistry, Lakehead University and Thunder Bay Regional Health Research Institute, 980 Oliver Road, Thunder Bay, On, P7B 6V4, Canada.

[e] School of Biotechnology and Health Sciences, Wuyi University, Jiangmen 529020, P.R. China; and International Healthcare Innovation Institute (Jiangmen), Jiangmen 529040, P.R. China.

‡ The authors contributed equally to this work.

* Corresponding author

E-mail: wing.leung.wong@polyu.edu.hk

List of contents

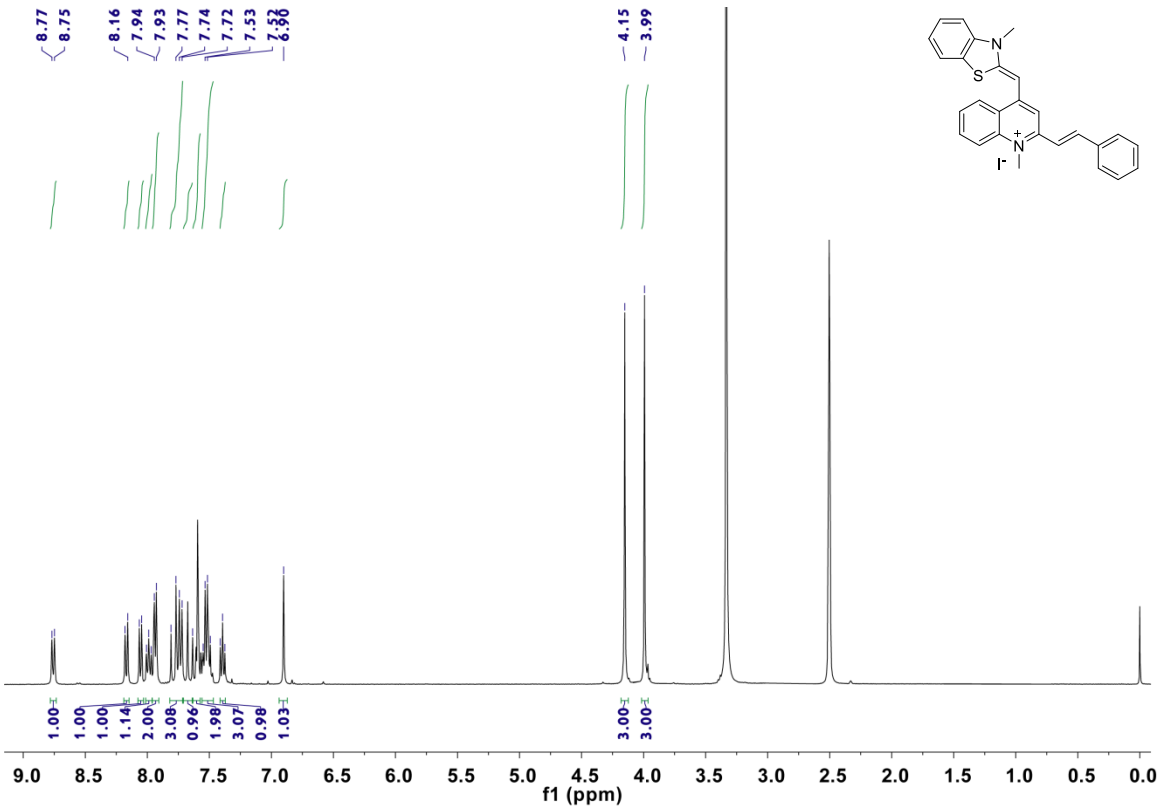

Figure S1a. [1]HNMR spectrum of ligand **1** (400 MHz, in DMSO-d_6)

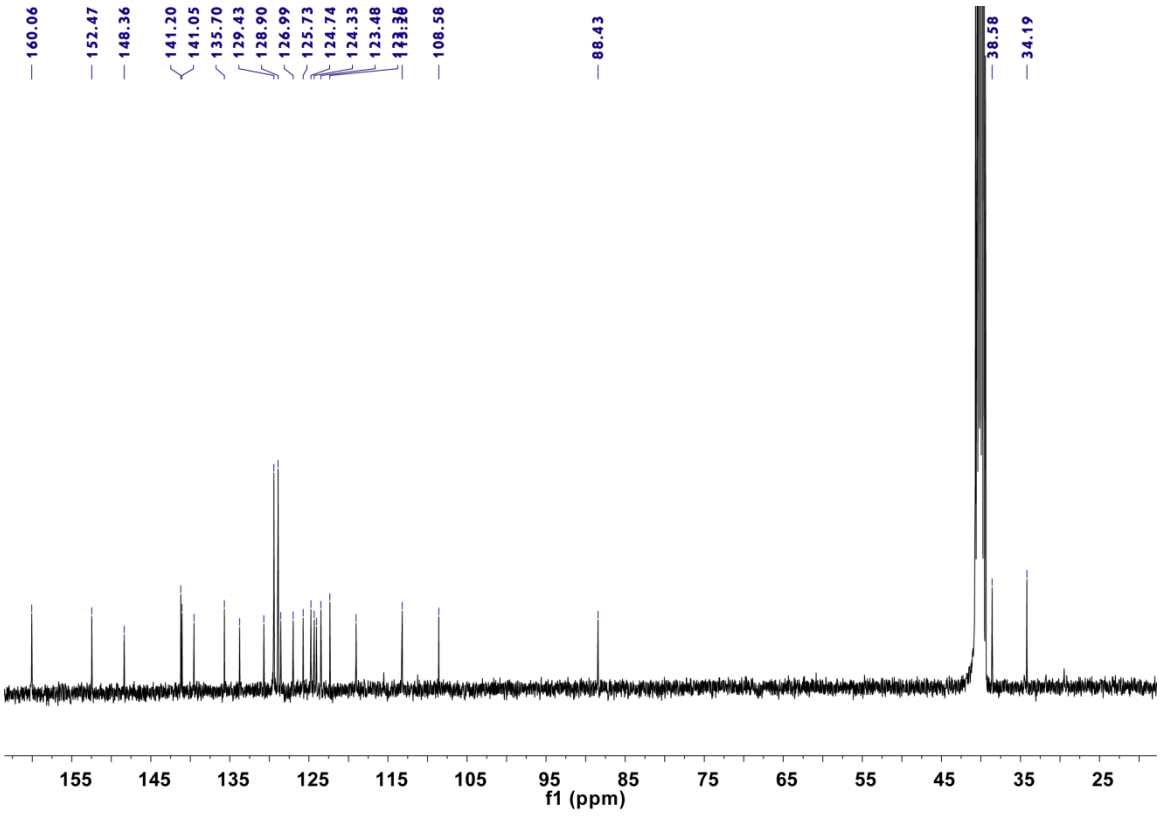

Figure S1b. [13]C NMR spectrum of ligand **1** (100 MHz, inDMSO-d_6)

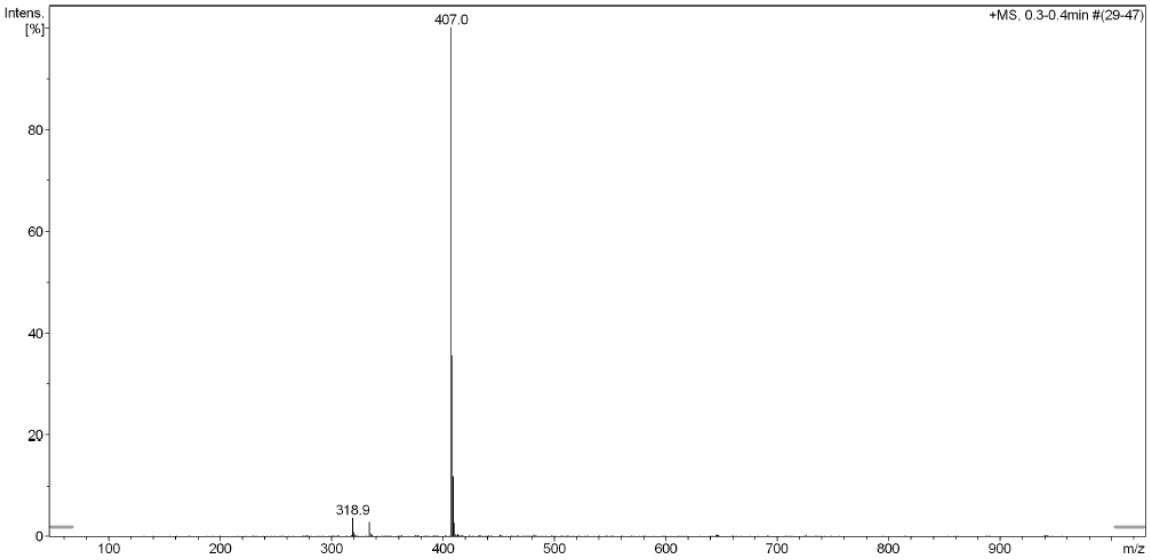

Figure S1c. ESI-MS analysis of ligand **1**

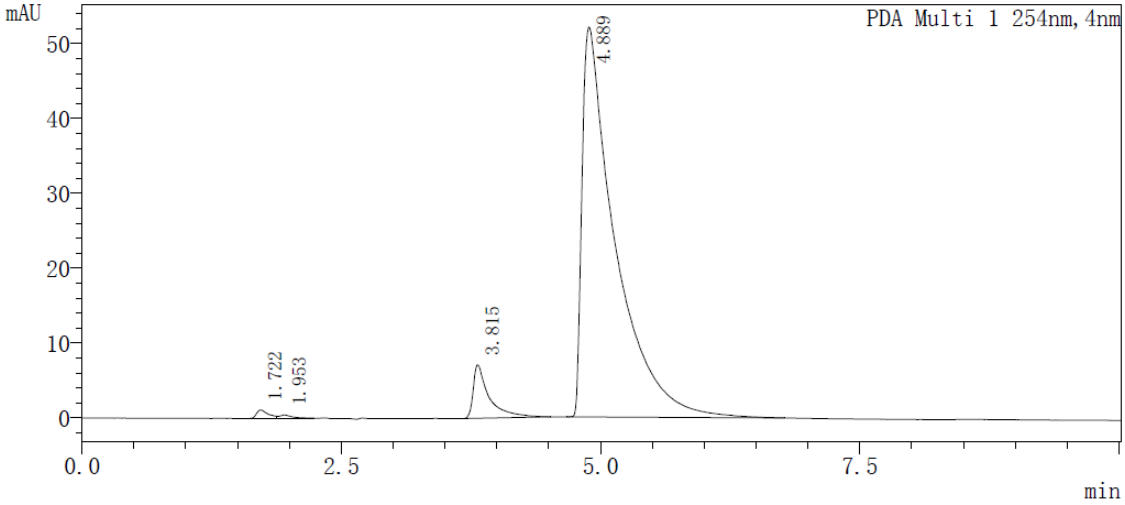

Figure S1d. HPLC analysis of ligand **1**

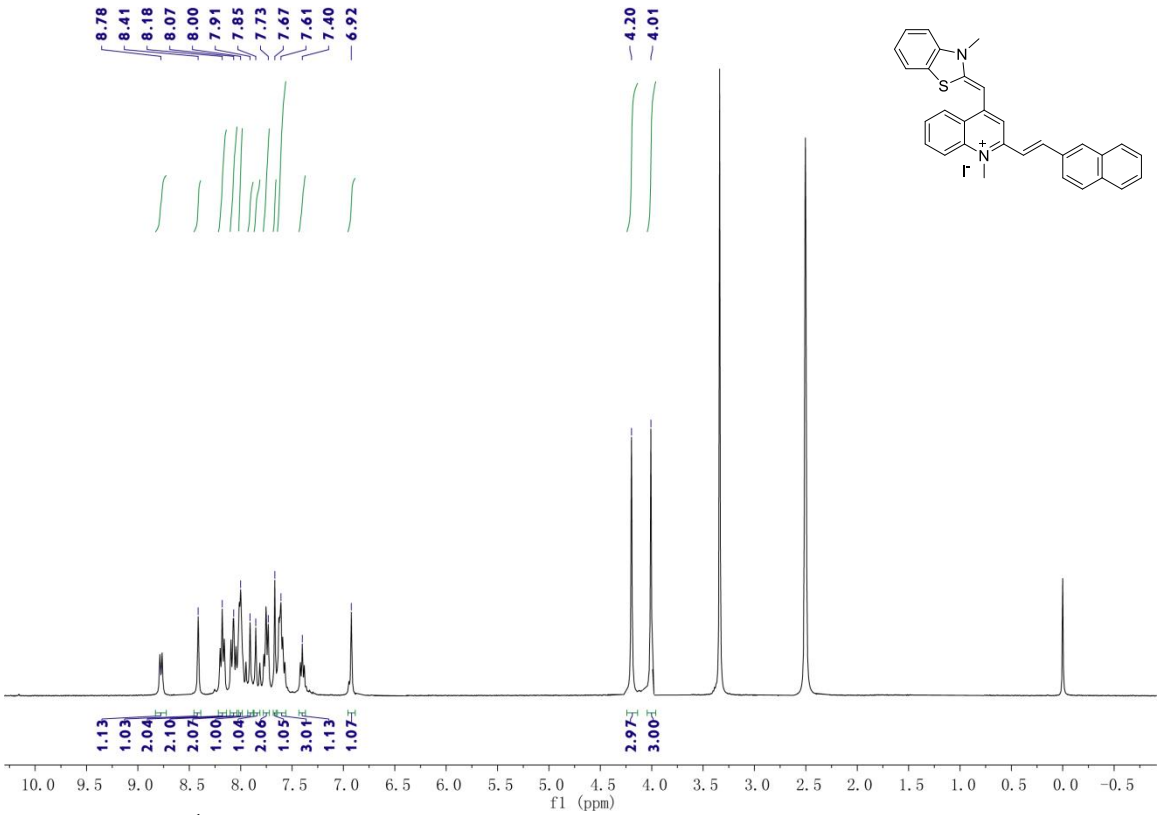

Figure S2a. ^{1}H NMR spectrum of ligand **2** (400 MHz, in DMSO-d_6)

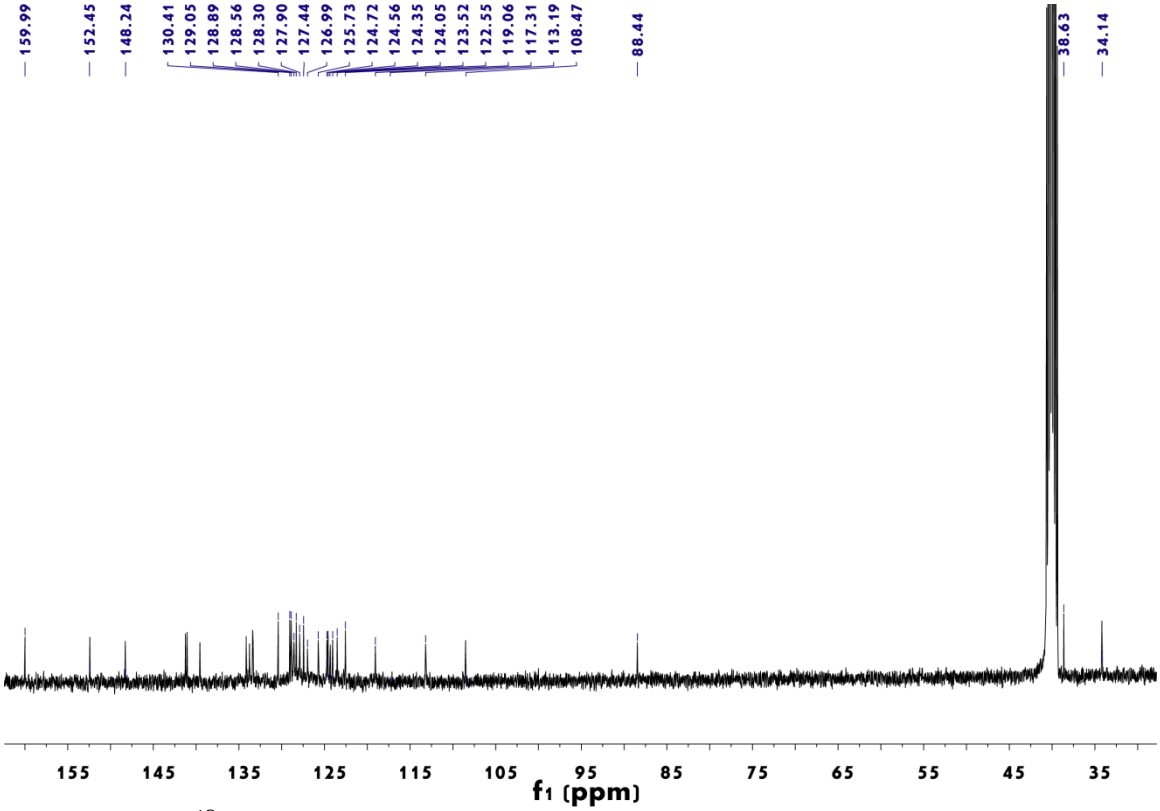

Figure S2b. ^{13}C NMR spectra of ligand **2** (100 MHz, in DMSO-d_6)

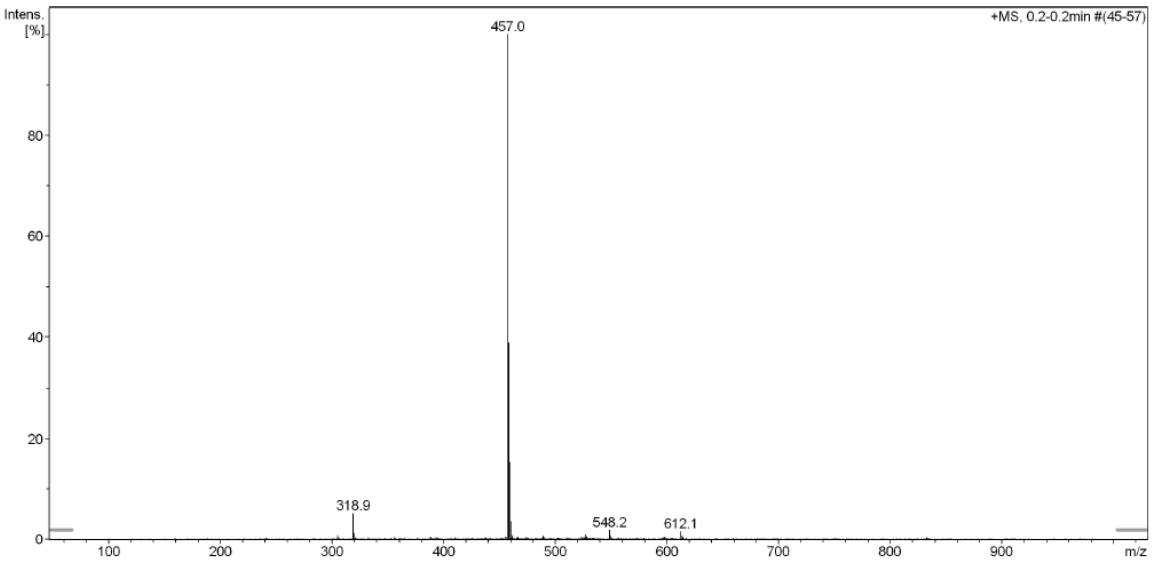

Figure S2c. ESI-MS analysis of ligand **2**

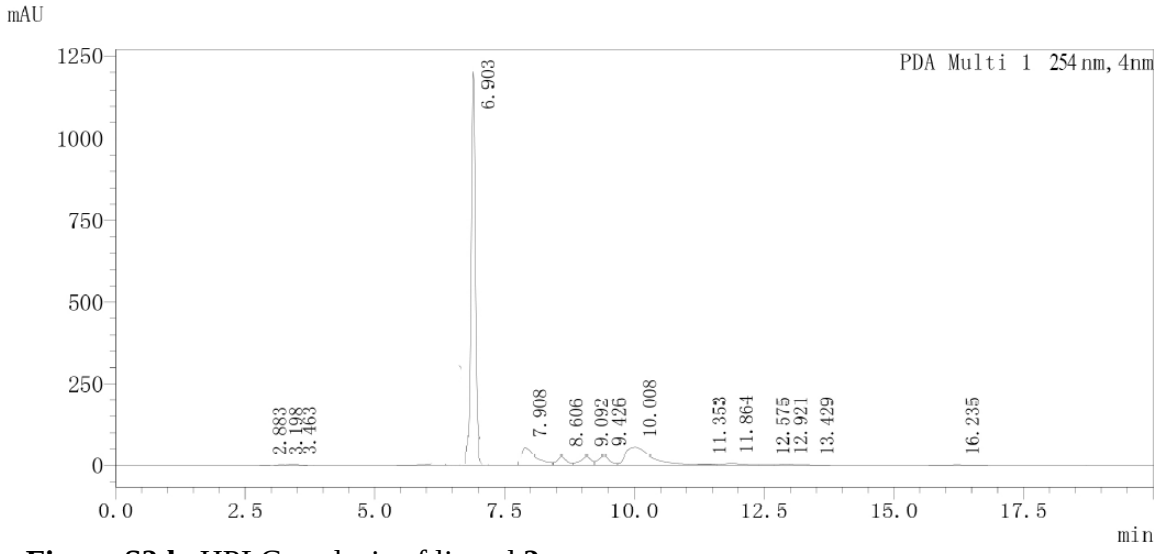

Figure S2d. HPLC analysis of ligand **2**

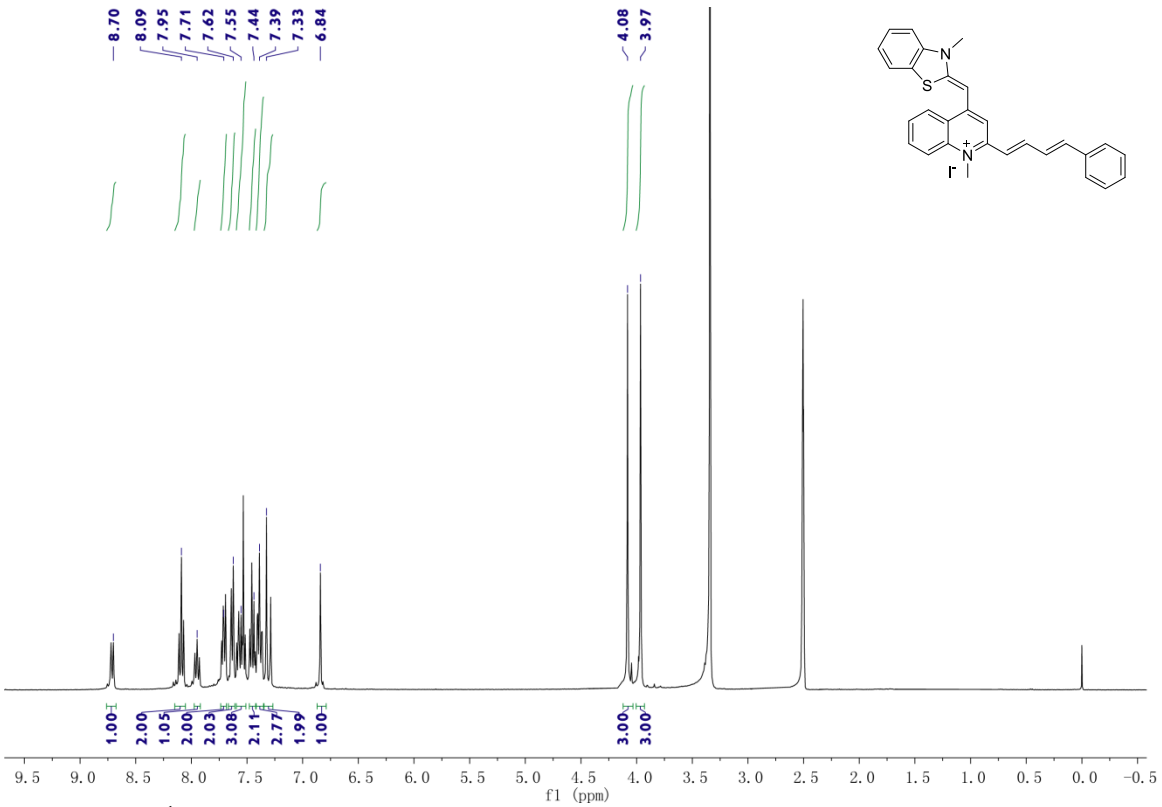

Figure S3a. ^{1}H NMR spectrum of ligand **3** (400 MHz, in DMSO-d_6)

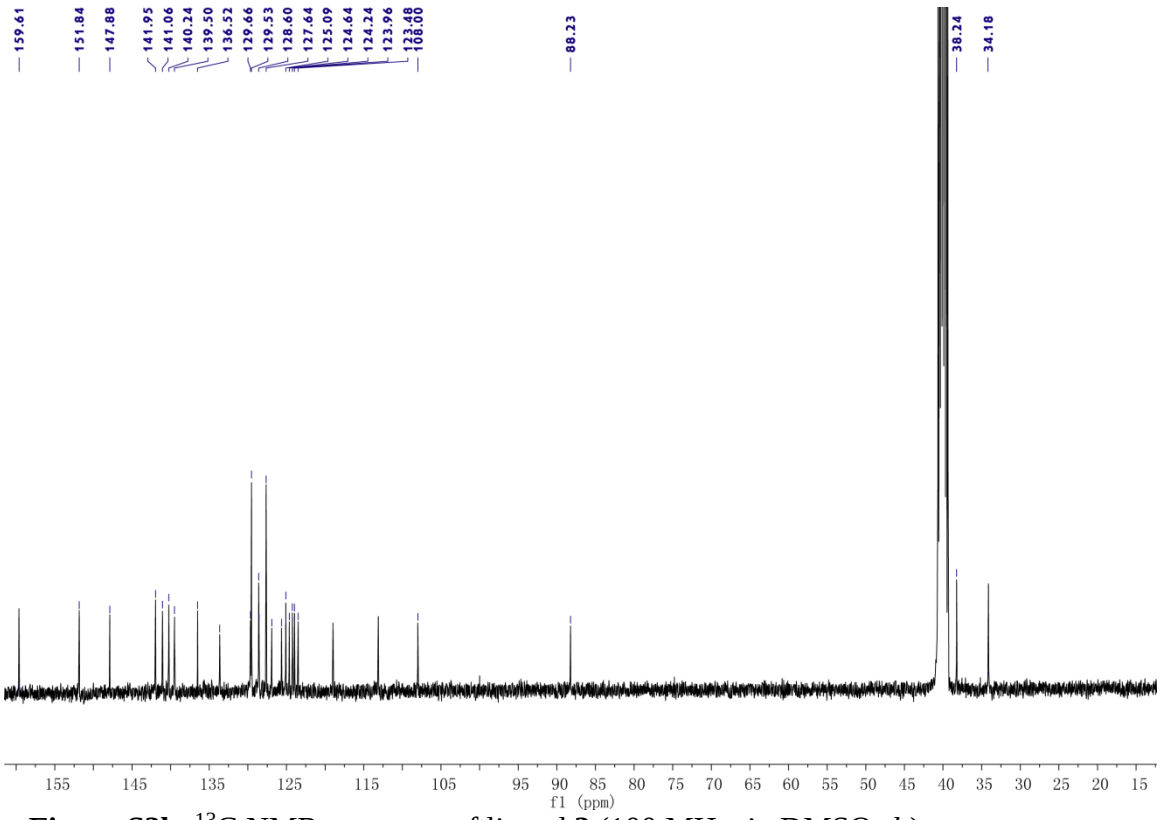

Figure S3b. ^{13}C NMR spectrum of ligand **3** (100 MHz, in DMSO-d_6)

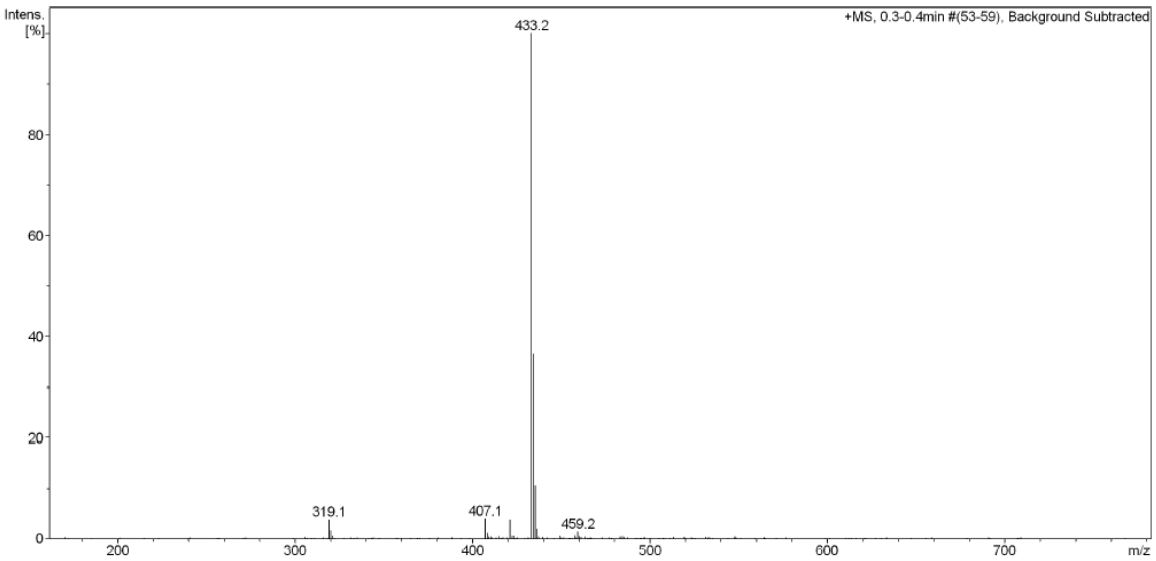

Figure S3c. ESI-MS analysis of ligand **3**

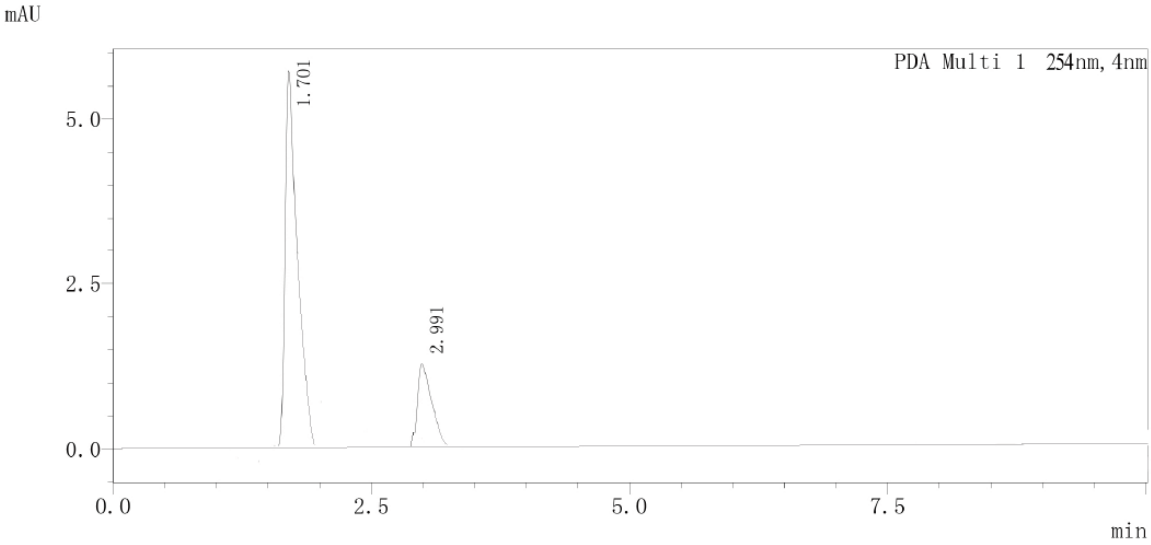

Figure S3d. HPLC analysis of ligand **3**

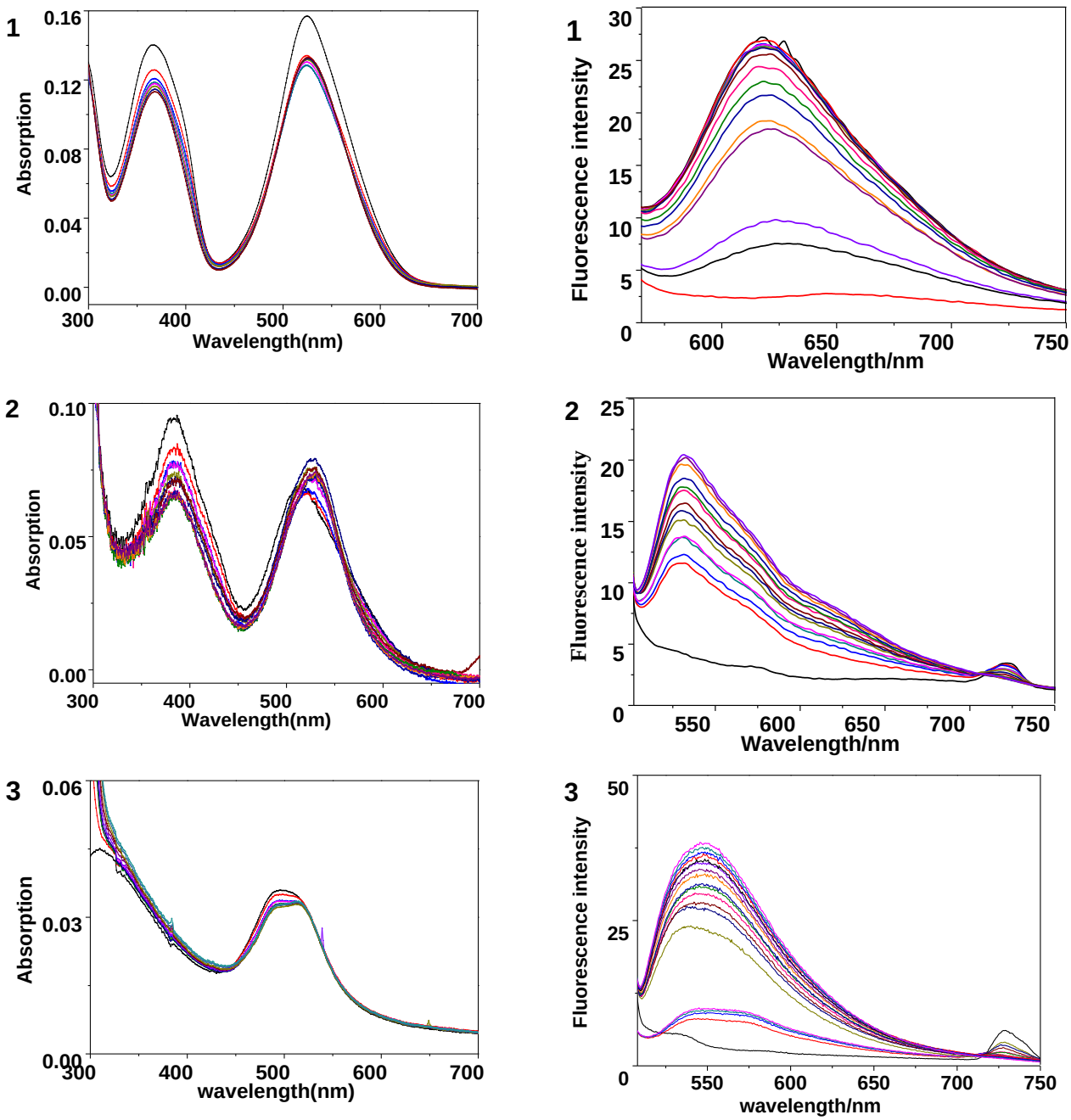

Figure S4. UV-vis and fluorescence titration spectra for ligands **1-3** with G-quadruplex DNA telo21. The final concentration of ligand was fixed at 5 μM in a Tris–HCl buffer containing 60 mM KCl. Measurements were taken after incubated for 10 min at 25 °C. (In the fluorescence titrations, the excitation wavelength was λ_{ex} = 510 nm and the fluorescence signal (λ_{em}) was recorded at emission maxima of ligands: **1**, λ_{em} = 620 nm; **2**, λ_{em} = 530 nm; **3**, λ_{em} = 550 nm.)

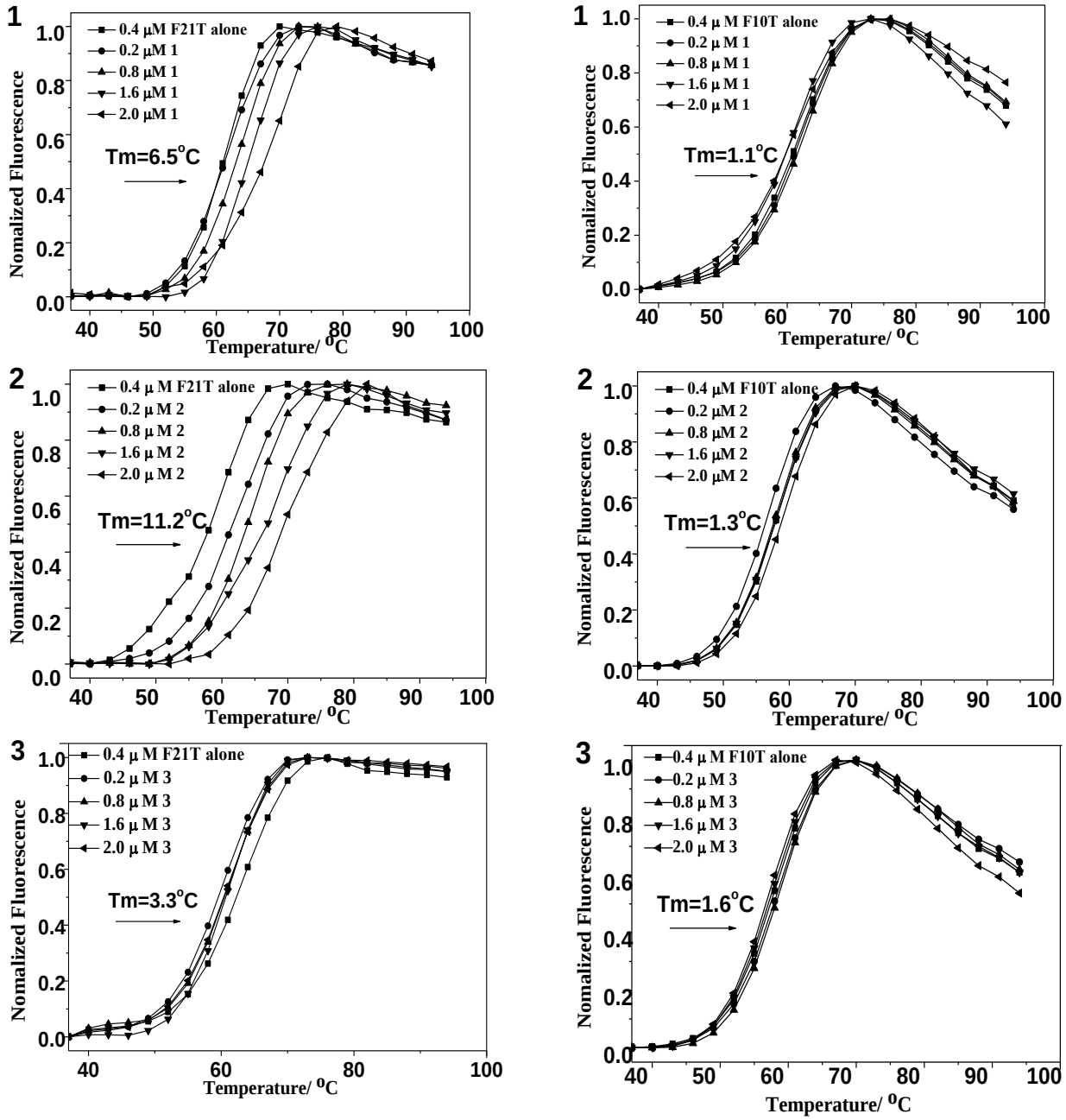

Figure S5. Normalized FRET melting curves of G-quadruplex F21T (0.4 μM) with the addition of different concentration of the DNA binding ligands **1-3** (0.2–2.0 μM) in 10 mM Tris–HCl, 60 mM KCl, pH = 7.4.

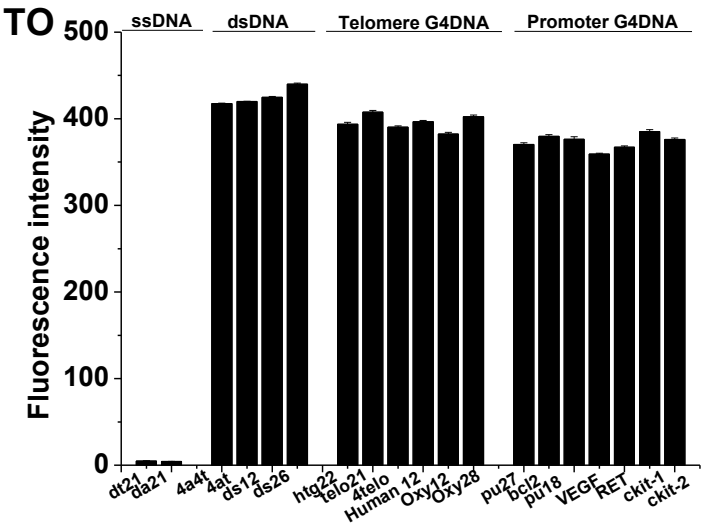

Figure S6. Fluorescence intensities at 630 nm (λ_{ex} = 475 nm) of thiazole orange with different nucleic acids in Tris–HCl buffer containing 60 mM KCl. Single-stranded DNA: da21, dt21; duplex DNA: 4a4t, 4at, ds12, and ds26; telomere G-quadruplex DNA: htg22, telo21, 4telo, human 12, oxy12, and oxy28; promoter G-quadruplex DNA: bcl2, ckit-1, ckit-2, Pu27, Pu18, RET and VEGF. Concentration of dye was 5 μM and DNA concentration was 10 μM. Results were adopted from [1] for comparison purpose only.

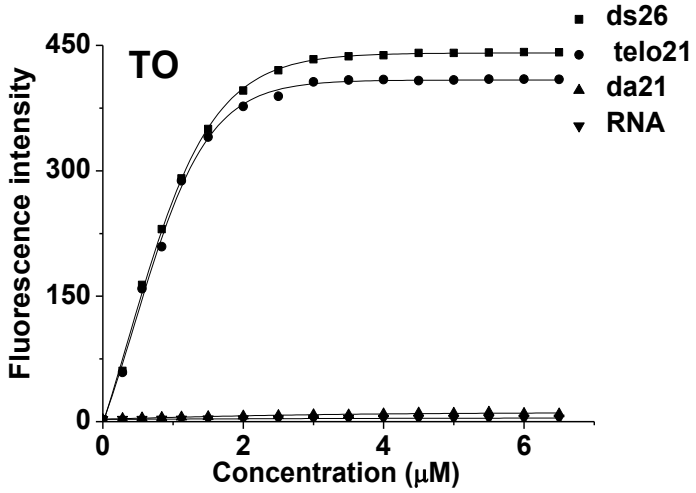

Figure S7. Equilibrium binding isotherms of thiazole orange with representative nucleic acids (ssDNA: da21, dsDNA: ds26, G4-DNA: telo21, and RNA) at various concentrations. The concentration of dyes was 5 μM in Tris–HCl buffer containing 60 mM KCl. Fluorescence signal was measured at 630 nm (λ_{ex} = 475 nm) at 25 °C. Results were adopted from [1] for comparison purpose only.

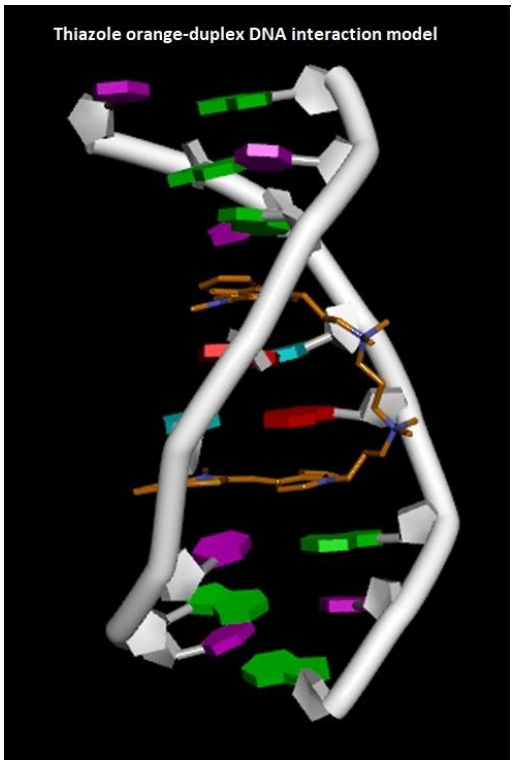

Figure S8. Molecular docking study of thiazole orange interacted with duplex DNA. The result was adopted from [1] for comparison purpose only.

Table S1. Sequences of oligonucleotides used in the present study

Abbreviation	Sequence (5' to 3')	Structure/origin
da21	AAAAAAAAAAAAAAAAAAAA	single-stranded
dt21	TTTTTTTTTTTTTTTTTTTT	single-stranded
4a4t	AAAATTTT	Duplex
4at	ATATATATATAT	Duplex
ds12	GCGCAATTGCGC	Duplex
ds26	CAATCGGATCGAATTCGATCCGATTG	Duplex
htg22	AGGGTTAGGGTTAGGGTTAGGG	Telomere G-quadruplex
oxy28	GGGGTTTTGGGGTTTTGGGGTTTTGGGG	Telomere G-quadruplex
telo21	GGGTTAGGGTTAGGGTTAGGG	Telomere G-quadruplex
oxy12	GGGGTTTTGGGG	Telomere G-quadruplex
Human12	TTAGGGTTAGGG	Telomere G-quadruplex
4telo	GGGTTAGGGTTAGGGTTAGGGTTAGGGTTAG	Telomere G-quadruplex
bcl2	GGGCGCGGGAGGAAGGGGGCGGG	Promoter G-quadruplex
ckit1	AGGGAGGGCGCTGGGAGGAGGG	Promoter-G-quadruplex
ckit2	GGGCGGGCGCGAGGGAGGGG	Promoter G-quadruplex
pu27	TGGGGAGGGTGGGGAGGGTGGGGAAGG	Promoter G-quadruplex
pu18	AGGGTGGGGAGGGTGGGG	Promoter G-quadruplex
VEGF	GGGGCGGGCCGGGGGCGGGG	promoter G-quadruplex
RET	GGGGCGGGGCGGGGCGGGGG	Promoter G-quadruplex
RNA	16*S*- and 23*S*-Ribosomal from *E. coli*	Duplex
F21T	FAM-(G_3[TTAGGG]$_3$)-TAMRA	Telomere G-quadruplex
F10T	FAM-TATAGCTA-HEG-TATAGCTATAT-TAMRA	Duplex

Table S2. The binding stoichiometry and the parameters of A and Q calculated for the fluorimetric titrations with ligands and telo21 G-quadruplex DNA.

Parameters	Ligand		
	1	**2**	**3**
A	81.05	64.36	106.36
Q	25.48	20.45	38.05
n *(binding stoichiometry)*	**0.92**	**0.95**	**1.06**

With the data obtained from fluorimetric titrations, the binding constants were analyzed according to the independent site model by nonlinear fitting to the following equation [2,3]:

$$F/F_0 = 1+(Q-1)/2\{A+1+x-[(x+1+A)^2-4x]^{1/2}\}$$

Where F_0 is the fluorescence intensity of ligands **1, 2** and **3** in the absence of DNA;

F_{max} is the fluorescence intensity upon saturation of DNA;

$Q = F_{max}(F_0)^{-1}$;

$A = (K_{eq}C_{dye})^{-1}$ and

$x = nC_{DNA}(C_{dye})^{-1}$;

n is the putative number of binding sites on a given DNA matrix.

The parameters, Q and A, were obtained via the Levenberg−Marquardt fitting routine in the Origin 8.5 software, whereas *n* was varied to obtain the best fit.

Reference:

1. Y.-J. Lu, Q. Deng, J.-Q. Hou, D.-P. Hu, Z.-Y. Wang, K. Zhang, L.G. Luyt, W.-L. Wong, C.-F. Chow, Molecular engineering of thiazole orange dye: Change of fluorescent signaling from universal to specific upon binding with nucleic acids in bioassay, ACS Chem. Boil., 11 (2016) 1019-1029.
2. F.H. Stootman, D.M. Fisher, A. Rodger, J.R. Aldrich-Wright, Improved curve fitting procedures to determine equilibrium binding constants, Analyst, 131 (2006), 1145-1151.
3. X. Xie, B. Choi, E. Largy, R. Guillot, A. Granzhan, M.P. Teulade-Fichou, Asymmetric Distyrylpyridinium Dyes as Red-Emitting Fluorescent Probes for Quadruplex DNA, Chem. Eur. J., 19 (2013) 1214-1226.